공학박사 학위논문

Experimental and numerical analysis for evaluating tool wear in cold stamping of ultra-high strength steel sheets

초고장력강판의 냉간성형의 금형 마모 평가를 위한 실험적 수치적 해석

2022 년 8 월

서울대학교 대학원

재료공학부

방 준 호

Experimental and numerical analysis for evaluating tool wear in cold stamping of ultra-high strength steel sheets

지도 교수 이 명 규

이 논문을 공학박사 학위논문으로 제출함
2022 년 8 월

서울대학교 대학원

재료공학부

방 준 호

방준호의 공학박사 학위논문을 인준함

2022 년 8 월

위 원 장 한 흥 남 (인)

부위원장 이 명 규 (인)

위 원 강 승 균 (인)

위 원 송 정 한 (인)

위 원 이 진 우 (인)

Abstract

The body of an automobile must be lightweight and crash-worthy. The use of advanced high-strength steel reduces the manufacturing cost for automobile body and improves energy absorption during an impact. However, increasing the strength of the steel sheet results in a variety of issues related to tool wear due to a higher forming pressure in the sheets than that in the conventional low-strength steel sheets. Therefore, systematic wear experimentation and prediction procedure are required to quantify the extent of tool wear during the press forming process. This study aims to develop a methodology for quantifying the wear of a sheet metal forming tool using experimental databases and a wear simulation procedure capable of predicting the nonlinear wear behavior of stamping tools in reduced computational time. A progressive die set is used to enable continuous sheet metal stamping at a consistent work rate and designed to conduct the wear test systematically, saving both time and cost. The testing machine is capable of testing four different types of punches simultaneously under a variety of tooling and process parameters, such as different tool materials, punch shapes, and coating conditions. The punches used in the wear test are designed to mimic the curvature geometry of the stamping tool used to manufacture the

automotive components. The wear depth, roughness, and surface imaging of the tool, as well as the product roughness are all used for tool wear evaluation in the sheet metal forming process. The wear depth of the punch is close to 0, and the roughness of the punch is also comparable to that of the as-produced prior to failure. When severe wear occurs, the depth of the wear and roughness of the punch rapidly increase. Prior to failure, micro-scratches on the punch surface do not degrade the punch quality. However, worn punches develop a very rough surface on the stamped product. Wear of coated tool is caused by the fretting wear mechanism when stamping uncoated steel sheets. By referring to the measured wear database, it was confirmed that the proposed methodology for wear testing and measurement in the sheet metal forming process is suitable for quantitatively and qualitatively evaluating the wear lifetime, and analyzing the wear characteristics and mechanism, as well as developing a reliable wear prediction model. To capture the nonlinear wear behavior with respect to strokes, a nonlinear equation from a modified form of Archard's wear model was constructed based on the wear test results. The scale factor, which represents the changes in wear properties with respect to wear depth, was utilized in the wear simulation to avoid the update of geometry from the previous iteration of wear simulation. By formulating a wear coefficient of Archard's wear model as a function of strokes and

implementing it into the scale factor of wear simulation, the nonlinear wear behavior of the stamping tools could be estimated. Therefore, the proposed simulation method is efficient in terms of computational time because it does not need to perform geometry updates.

Keywords: Sheet metal forming, Ultra-high strength steel, Tool wear, Fretting wear, Tool wear test, Progressive die, Wear simulation

Student number: 2019-39333

Contents

List of Tables

List of Figures

1. Introduction

1.1. Research background

In recent years, the acceleration of the development of eco-friendly vehicles such as electric vehicles and hydrogen vehicles has led to a growing demand for lightweighting of the vehicle body to improve mileage. In addition, for passenger safety and the protection of batteries and fuel cells, many efforts have been made to secure the crashworthiness of the vehicle body. Automobile body weight can be reduced by using lightweight materials such as advanced high-strength steel (AHSS), aluminum alloys, magnesium alloys, glass-fiber composites, and carbon-fiber composites. Although AHSS results in the least weight reduction among these lightweight materials, it is relatively inexpensive to produce AHSS automotive body components, as shown in Fig. 1-1 [1–3]. Furthermore, a vehicle structure composed of AHSS showed outstanding crash safety performance in a simulation of three crash tests: frontal wall impact, side barrier impact, and roof strength tests [4]. Automakers have increased the proportion of AHSS used in vehicle structures to reduce the cost and meet safety regulations, as shown in Fig. 1-2 [5]. Moreover, to reduce the manufacturing cost of mass-produced vehicle components, the cold forming process is generally used. However, the cold

forming of AHSS sheets is relatively vulnerable to tool wear. The higher strength characteristics of AHSS sheets in comparison with conventional steel sheets may generate premature tool wear, which leads to many problems such as reduced productivity, reduced product quality, and increased maintenance cost. Therefore, in the mass production of automobile components using AHSS sheets, the investigation of the tool wear resistance is essential for efficient process management.

Material	Weight Reduction (%)	Relative Cost per Part[13] (%)
Advanced high-strength steels (AHSS)	15–25	100–150
Glass fiber composites	25–35	100–150
Aluminum	40–50	130–200
Magnesium	55–60	150–250
Carbon-fiber composites	55–60	200–1000

Fig. 1-1. Weight reductions and cost obtained by using lightweight materials in automobile structures [3].

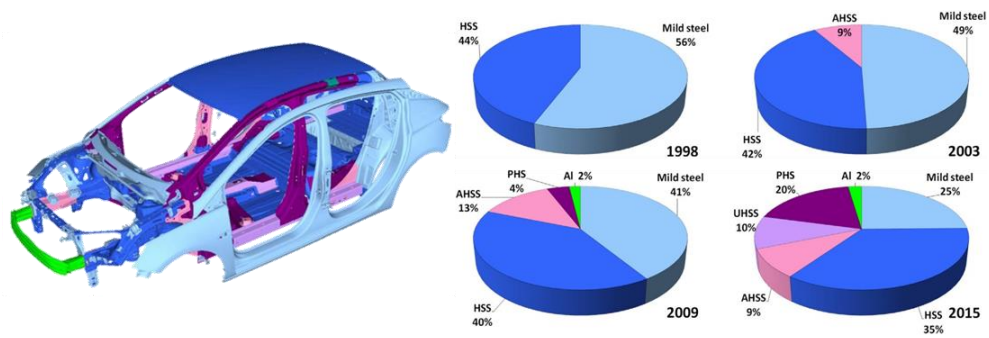

Fig. 1-2. Chronological evolution of automobile structure depicted in terms of portions of used materials [5].

Consistent efforts to improve the strength of steel sheets that are used in automobile fabrication have aggravated the tool wear problems. A countermeasure to increase tool wear resistance is required to manage the mass production process. Numerous studies have been conducted to find methods to extend the tool wear lifetime. Pereira et al. [6] investigated the effect of the machining error of the die profile shape on the tool wear in sheet metal forming. A small and localized change of the die radius profile shape has a significant effect on the tool-life reduction. Podgornik and Jerina [7] confirmed the effect of surface roughness on galling resistance for coarse and fine ground forming tools with a monolayer physical vapor deposition (PVD) TiN hard coating and multilayer plasma-assisted chemical vapor deposition (PACVD) W-doped DLC coating under dry sliding conditions. Podgornik et al. [8] investigated the influence of the surface preparation condition of forming tool steel with PVD coatings (TiN, TiB_2, TaC, and WC/C) on galling properties. Gonzalez-Pociño et al. [9] confirmed the heat treatment parameters (quenching, tempering, and nitriding process) that significantly affect adhesive wear resistance through an experiment in which these parameters were deliberately changed. Ogunbiyi et al. [10] suggested that the wear performance of Inconel 738 low carbon compoistes could be enhanced with the addition of grapheme nanoplatelets. Büyükkayacı et al. [11]

investigated the influence of mechanical alloying time on wear resistance for Fe–Cu–C alloys. Sıralı et al. [12] determined the effect of grain size reduction of titanium–zirconium–molybdenum alloys obtained with addition of Ti on wear performance. Woodward et al. [13] investigated the sliding wear response of G320 grey cast iron in different microstructure conditions resulting from quench and temper heat treatment. Hou et al. [14] evaluated the galling behaviors in sheet metal forming under various tool conditions with respect to hardness, surface roughness, and coating. Ghiotti and Bruschi [15] and Cora et al. [16] investigated the effect of various coating techniques on wear resistance by using a wear test system imitating stamping process conditions. van der Heide et al. [17] evaluated the effects of various lubricated conditions on galling by using a slider-on-sheet tribometer. Groche and Christiany [18] examined the wear evolution of various tool materials by assessing tool roughness and wear volume during strip drawing of AHSS sheets. Zhao et al. [19] evaluated microstructure, mechanical properties and wear resistance of Ti(C,N)-based cermet with respect to different WC additions. Thus, the above-mentioned studies demonstrate that by controlling various process and tooling parameters such as surface coating, heat treatment, and surface finish, the tool's wear resistance can be effectively increased. Numerous studies aimed at extending the tool life have reported on various

methods that can be used to effectively delay the wear. However, tool wear is influenced by a number of process parameters during the stamping of the automotive body, including tool geometry, surface roughness, tool materials, and coating conditions. Thus, for the efficient management of automobile mass production, a reasonable wear test and prediction method that takes various process parameters into account is required.

1.2. Wear testing methods

An experimental method to estimate the wear resistance of a tool can enable the prediction of the tool lifetime and facilitate effective management for stamping tools in mass production. Therefore, extensive experimental methods have been proposed for estimating the wear of stamping tools in the sheet metal forming process.

The wear behavior of various coated tools have been previously evaluated using a pin-on-disk test, as shown in Fig. 1-3 [15, 20–24]. However, it has the disadvantage that the pin repeatedly contacts the already worn sheet material surface. To compensate for this shortcoming, slider-on-sheet–type wear test methods [17, 25–29], in which the tool comes into contact with the virgin sheet material, have been used, as shown in Fig. 1-4. However, the wear test

methods described above do not reflect the deformation modes encountered in automotive sheet metal forming. Thus, representative wear tests considering the actual conditions prevalent in automotive sheet metal forming were performed, such as bending-under-tension (see Fig. 1-5) [30–34], and U-bending (see Fig. 1-6) [6, 35–39]. However, they are cumbersome and uneconomical to perform for stamping tools with a large number of strokes.

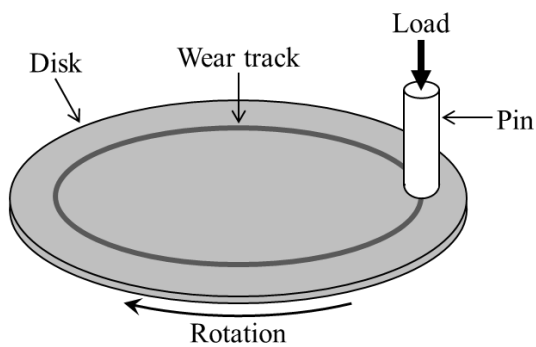

Fig. 1-3. Schematic illustration of the pin-on-disk test.

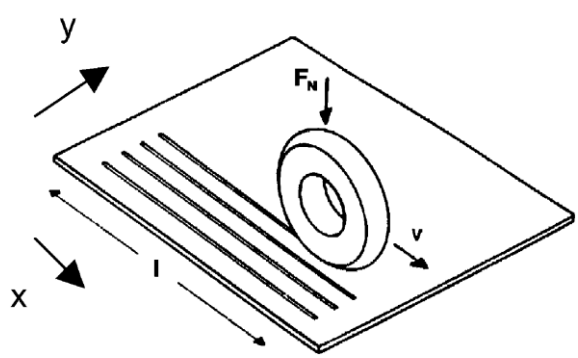

Fig. 1-4. Schematic illustration of the slide-on-sheet−type test [17].

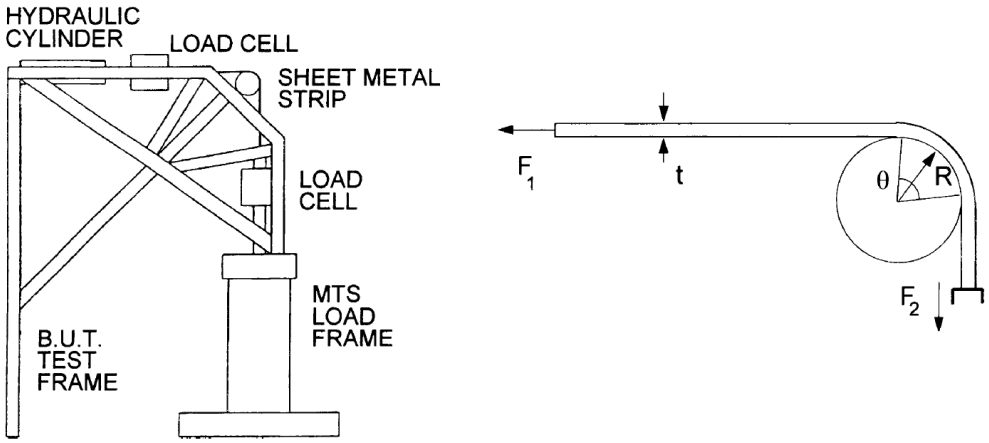

Fig. 1-4. Schematic illustration of the bending-under-tension test [32].

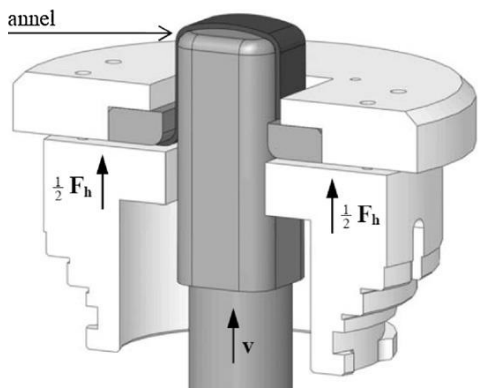

Fig. 1-5. Schematic illustration of the U-bending test [6].

The Auto/Steel Partnership proposed a method for testing the wear of stamping tools in the press forming process, which is efficient, economical, quick, and convenient, as shown in Fig. 1-6 [40]. The layout of the applied progressive die set capable of conducting continuous wear tests is depicted in Fig. 1-6(a). As shown in Fig. 1-6(b), the progressive die set was designed to evaluate various combinations of tool materials and coatings in a single press stroke. It reported on a qualitative investigation of the die wear resistance of

various tooling materials and coatings during the stamping operation of the DP1180 steel sheet, as shown in Fig. 1-6(c). Thus, they revealed that qualitative wear analysis can be used to determine the approximate time of tool wear initiation and to compare the relative wear resistance of various tools. However, quantitative identification and evaluation of wear characteristics, mechanisms, and evolutionary behaviors for a variety of tooling and process parameters, such as tool materials, coatings, surface finish, and sheet materials, are limited. When tool wear in the press forming process is quantified, the specific wear mechanism affecting the tool wear can be understood, which allows an accurate analysis of the initiation and development of tool wear. When designing a tool, significant wear factors can be eliminated in advance, and the appropriate tool conditions can be chosen. Thus, it can be used as a guideline for tool design to extend the tool lifetime. The surface quality of the product is directly related to the tool's surface condition. Therefore, it is critical to identify the tool's surface condition for the effective management of the mass production process. Quantifying the tool's wear can aid in increasing productivity and lowering maintenance costs. Moreover, a trustworthy wear database is critical for developing an accurate equation for predicting tool lifetime. As a result, systematic wear

experimentation and evaluation processes should be developed to quantify the extent of tool wear during the press forming process.

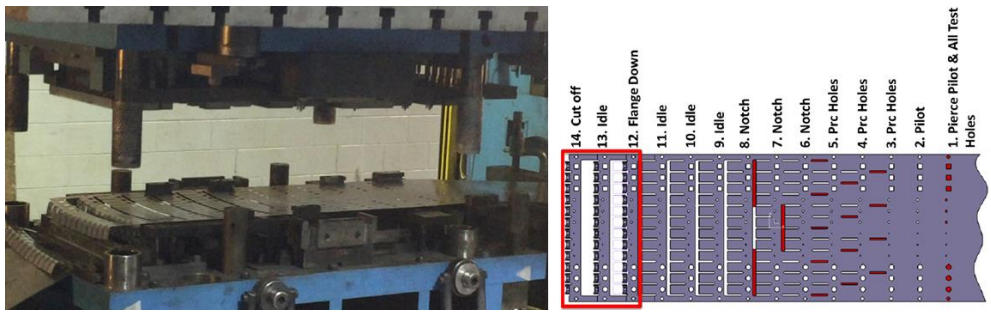

(a)

	12	11	10	9	8	7	6	5	4	3	2	1
Die Mater.	CC1	S0050A	S0050A	S2333	TD2	TD2	DC53	TD2	TD2	T44	CC1	D6510
Coating	HVOF MPD	Cr Plate over Ion Nitride	Cr Plate	PVD Duplex CrN	Concept	Cool Sheet	PVD Duplex CrN	PVD Duplex CrN	PVD Duplex CrN	PVD Duplex CrN	PVD Duplex CrN	PVD Duplex CrN
Hardness (Rc)	54-58	38-43	54-58	40-45	55-60	55-57	55-60	55-57	55-58	44-46	38-42	54-58

	12	11	10	9	8	7	6	5	4	3	2	1
Die Mater.	D2 (NEW)	D2 (NEW)	D2 (NEW)		TD2 (NEW)						D2 (NEW)	D2 (NEW)
Coating	PVD Duplex CrN	PVD Duplex CrN	PVD Duplex CrN		Concept + Most						PVD Duplex CrN	PVD Duplex CrN
Hardness (Rc)	58-60	58-60	58-60		58-60						58-60	58-60

(b)

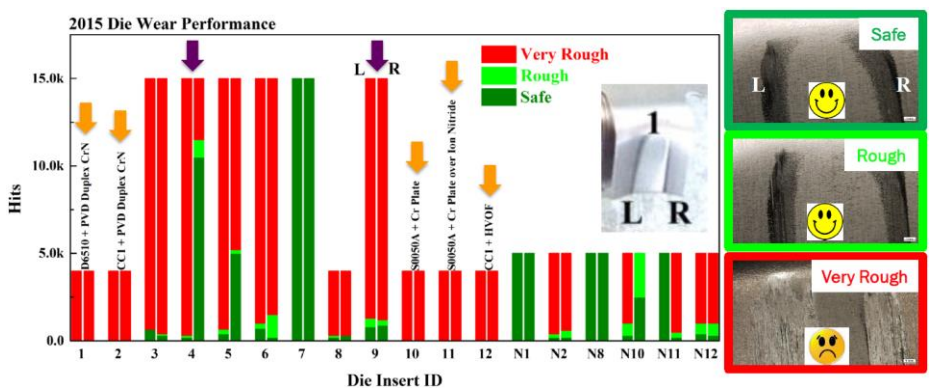

(c)

Fig. 1-6. A wear testing method for stamping tools using a progressive die set. (a) the layout of a progressive die set, (b) experimental combinations of tool materials and coatings, (c) qualitative evaluations of wear lifetime [40].

1.3. General wear simulation scheme

Although various experimental methods have been presented for evaluating the tool wear in sheet metal forming, the wear evaluation of the press forming tool still has limitations in that it entails significant cost, time, and human effort. To reduce the time required for tool wear prediction in sheet metal forming, several numerical simulation studies have been conducted on tool wear prediction. Hoffmann et al. [41] proposed a wear simulation scheme using Archard's wear equation to calculate the elemental wear, which is linearly proportional to the number of strokes. However, in sheet metal forming, the tool wear is nonlinear with respect to the number of strokes. Therefore, many efforts have been made to estimate the wear behavior of stamping tools reasonably and accurately. Ersoy-Nürnberg et al. [42] proposed a modified Archard's model with a variable wear coefficient with respect to the loading duration. The wear coefficient is a function of the accumulated wear work and is determined through deep-drawing experiments. Wang et al. [22] approximated the changes in wear coefficient during testing

by using pin-on-disk test results to reflect the variation of wear characteristics reasonably. The studies described above used a simulation scheme of updating the geometry based on changes to the geometry calculated from interactive iterations of forming and wear simulation, as shown in Fig. 1-7. A wear simulation calculates elemental wear using contact-related information obtained from a forming simulation. The updated geometry from the wear simulation is used in the next forming simulation. These procedures are repeated until the desired iteration. Therefore, the conventional wear simulation scheme considering the geometry update requires substantial computational time to predict the wear of forming tools. In addition, because the studies described above evaluated only simple models, wear simulation for complex and large parts such as automobile components requires massive computational time. Therefore, it is necessary to establish a reasonable wear simulation process that takes less computational time and considers the nonlinear tool wear behavior in sheet metal forming.

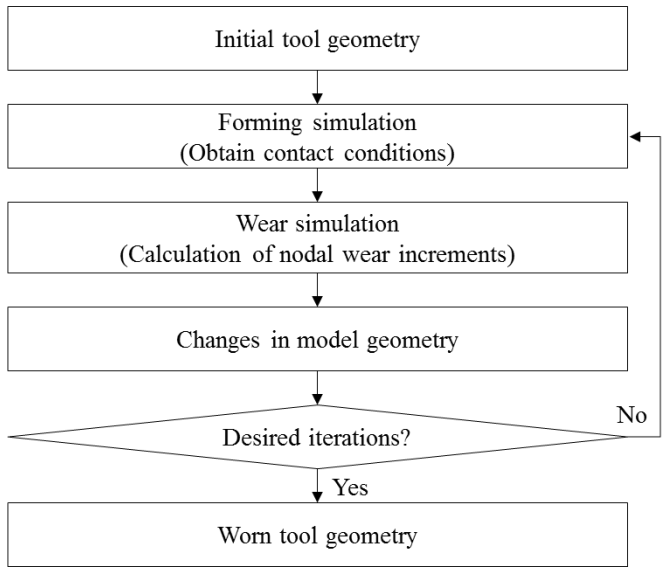

Fig. 1-7. General wear simulation scheme [22, 41–42].

1.4. Objective and scope

The first objective of this study is to develop a novel methodology for quantifying tool wear during the sheet metal forming process. To conduct a systematic wear test, a progressive die set is designed and used to evaluate the wear characteristics of four different types of punches in a single press stroke. The punches were subjected to wear tests under a variety of tooling and process parameters, including tool materials (STD-11, K340), punch shapes (R3.0 and R5.5), and coating conditions (PVD CrN and AlTiCrN coatings). The wear characteristics and behaviors of the tool were quantitatively examined based on the tool wear depth, tool roughness, and

product roughness. Further, using the tools' experimental wear databases, it was confirmed that the proposed methodology for wear testing and measurement in the sheet metal forming process is suitable for analyzing the wear characteristics and mechanism, as well as for developing a reliable wear prediction model. Additionally, the tensile strength of an UHSS sheet used in automotive manufacturing—an uncoated transformation induced plasticity (TRIP) steel sheet with a tensile strength of 1180 MPa, TRIP1180—was investigated.

The second objective of this study is to develop a wear simulation procedure capable of predicting the nonlinear wear behavior of stamping tools in reduced computational time. A nonlinear equation from a modified form of Archard's wear model was constructed based on the wear test results of a stamping process for different punch shapes (R3.0 and R5.5) and coating conditions (PVD CrN and AlTiCrN coatings). The scale factor, which represents the changes in wear properties with respect to wear depth, was utilized in the wear simulation to avoid the update of geometry from the previous iteration of wear simulation. By formulating a wear coefficient of Archard's wear model as a function of strokes and implementing it into the scale factor of wear simulation, the nonlinear wear behavior of the stamping tools could be estimated. Therefore, the suggested wear simulation method

can save computational time in the prediction of the nonlinear wear behavior of stamping tools.

2. Experimental setup for evaluating tool wear

2.1. Punch design

Contact pressure and sliding distance are critical parameters that determine the tool lifetime [22, 43]. Tool wear occurs most frequently in the region of the curvature where the contact pressure is concentrated and the sliding distance is large. Regions with small radius of curvature and high contact pressure experience high rate of wear. The wear test punch was designed to replicate the contact conditions encountered during the sheet metal forming process. Fig. 2-1 illustrates the examples of geometries for automotive components designed with UHSS sheets to ensure passenger safety. The smallest curvature radius in the automotive components is approximately 3.6 to 5.5 mm. Because these regions come into contact with the tool shoulder, a large sliding distance is also expected during forming. The detailed punch design for the wear test is shown in Fig. 2-2. To compare wear rates with respect to tool curvature radius, the punch radius was set to 3.0 mm and 5.5 mm, respectively, based on the curvature of the stamping tools used to manufacture the automotive parts so that wear was concentrated in the curvature region, as illustrated in Fig. 2-2(a) and (b). The punch was designed as an insert-type to allow the efficient replacement and examine the tool wear

characteristics of the worn-out punch. Thus, it was designed to facilitate the measurement of extent of wear of the punch radius and identify the wear behavior. Fig. 2-2(c) illustrates a schematic representation of the stamping process used in the wear test. A padding force was used to keep the blank in place during the stamping process. After several stampings, the designed punch slides and bends the blank, causing wear in the punch's tip region.

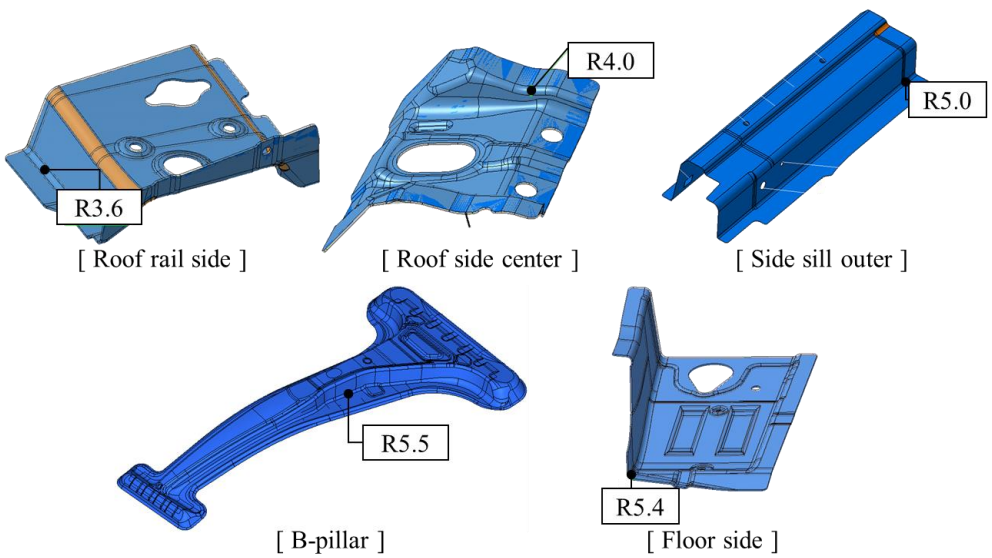

Fig. 2-1. Examples of automotive part geometries using UHSS sheets.

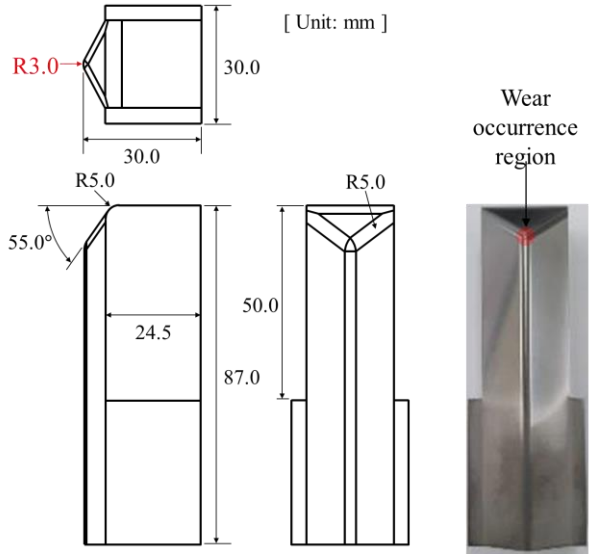
[Unit: mm]
R3.0
30.0
30.0
R5.0
55.0°
24.5
87.0
R5.0
50.0
Wear
occurrence
region

(a)

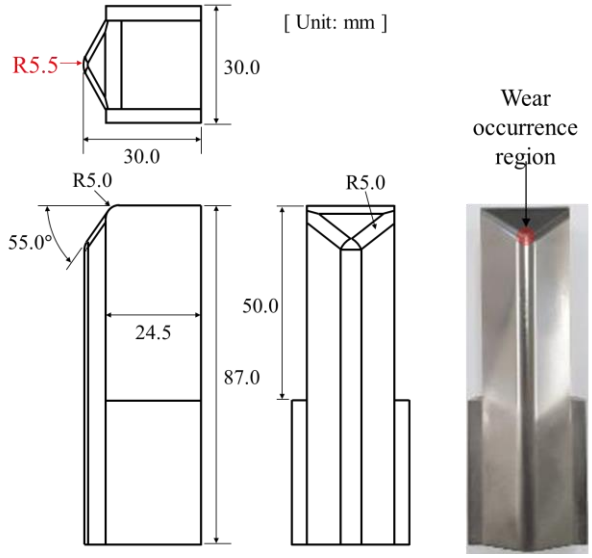
[Unit: mm]
R5.5
30.0
30.0
R5.0
55.0°
24.5
87.0
R5.0
50.0
Wear
occurrence
region

(b)

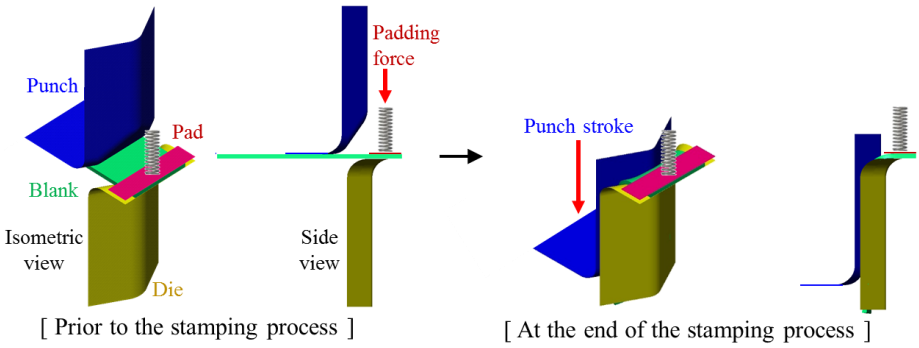

(c)

Fig. 2-2. Detailed design of tool wear test. (a) geometry and dimensions of punch with a radius of 3.0 mm, (b) geometry and dimensions of punch with a radius of 5.5 mm, (c) schematic representation of wear test.

2.2. Design of continuous wear test

Evaluating tool wear during the sheet metal forming process consumes significant time, sheet material, and labor. To address these shortcomings, this study developed an experimental setup capable of conducting continuous wear tests using the progressive stamping concept. Progressive stamping is a composite process that combines multiple metalworking operations into a single press stroke, allowing continuous sheet metal production and consistent work rates. The continuous wear test was conducted using a rolled steel coil, which is more efficient and economical than producing specimens because it conserves raw materials and eliminates the need for specimen

production. The layout of the applied progressive die set is depicted in Fig. 2-3. It was designed to evaluate the wear characteristics of four different types of punches simultaneously in a single press stroke, thereby reducing the time and cost associated with the wear test. As illustrated in Fig. 2-3(a)−(c), the piercing process uses the shearing tool (indicated in yellow) to create holes in the sheet. This is referred to as Operation 1 (OP1). These holes are used to secure the sheet metal in place and to allow it to enter the press system in 75 mm sections during the metalworking operation. OP2, OP4, and OP5 comprise the punching process, which utilizes the shearing tool to prepare a blank shape (indicated in purple) prior to the stamping process. Because of the contact between the sheet metal and stamping punch, the stamping process (OP7 and OP9) causes tool wear. The punch stroke is 35 mm. When four different types of punches are used in one operation, the operation load may become concentrated, resulting in a press system malfunction. As a result, the stamping process was divided into two operations to distribute the operation load. Between each operation, idle operations (OP3, OP6, and OP8) were added for further operation load distribution. Finally, the parting process (OP10) uses a shearing tool to separate the completed product from the sheet metal. Figure 2-3(d) illustrates a steel strip with the progressive intended metalworking operations of a die set.

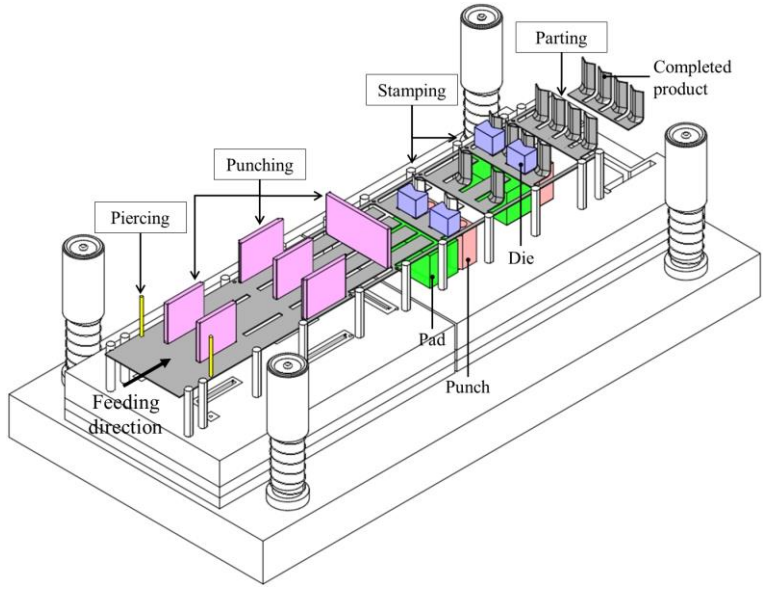
Parting
Completed product
Stamping
Punching
Piercing
Die
Pad
Punch
Feeding direction

(a)

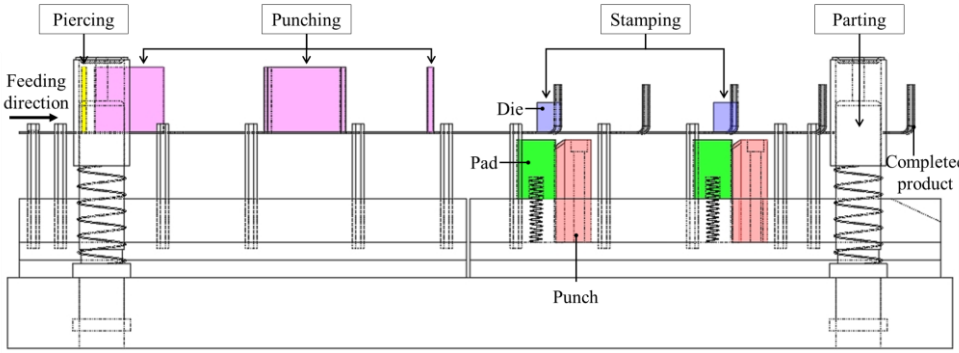
Piercing
Punching
Stamping
Parting
Feeding direction
Die
Pad
Completed product
Punch

(b)

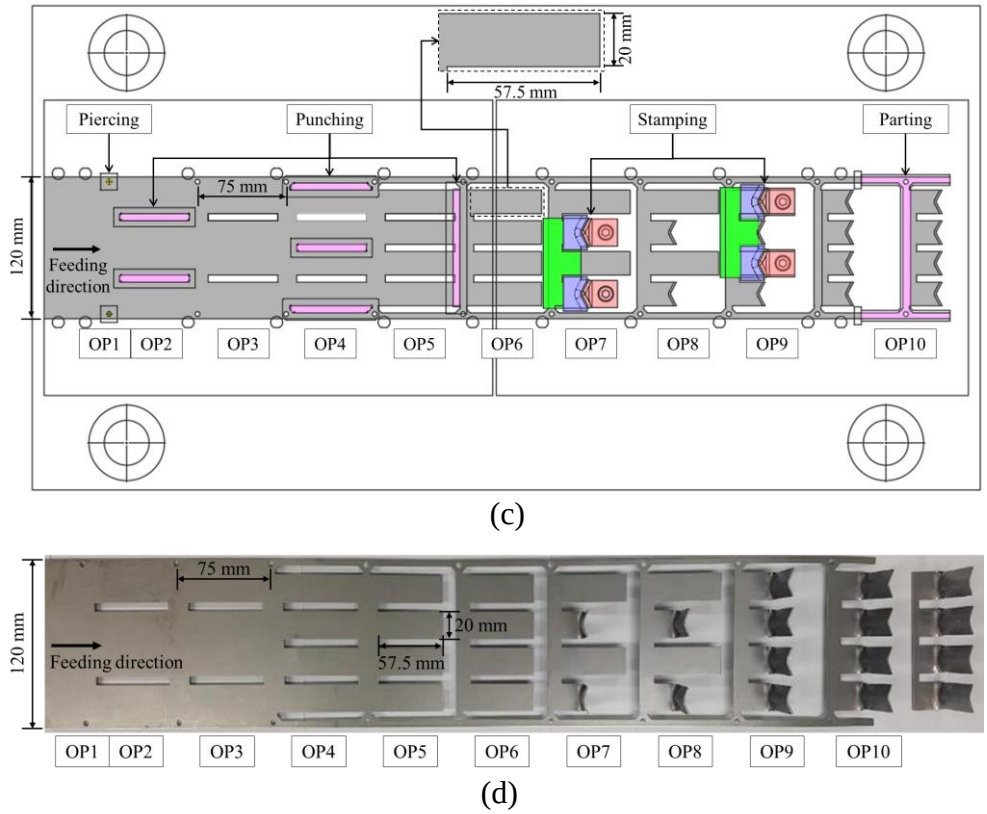

Fig. 2-3. The layout of a progressive die set for continuous tool wear tests. (a) isometric view, (b) side view, (c) top view, (d) steel strip

The apparatus used for the continuous wear test are depicted in Fig. 2-4. The uncoiler is a machine that is used to hold and supply the coil sheet during the press operation. The press system is equipped with a progressive die set. The automatic feeding system feeds the sheet metal into the progressive die set in 75 mm sections as the upper die of the progressive die set moves up.

When the upper die is lowered, the specified metalworking operations are carried out, and the desired shaped products are finally produced.

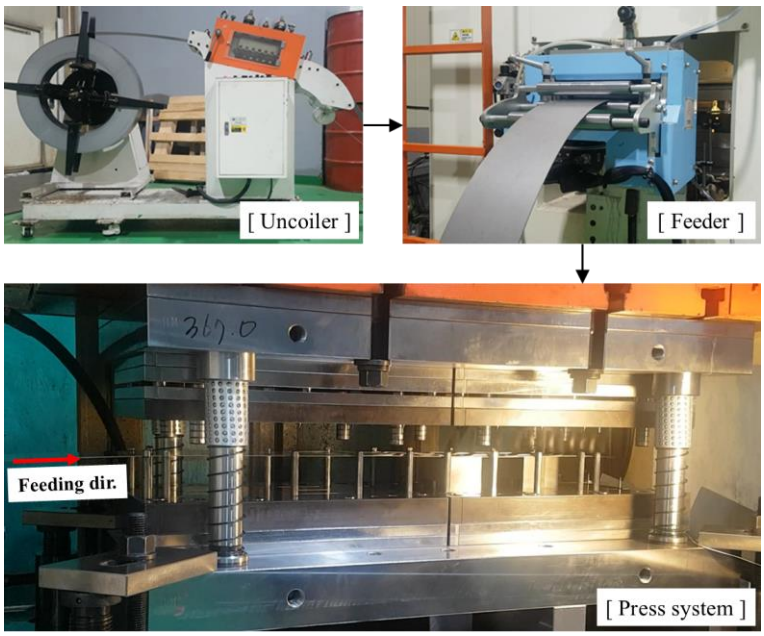

Fig. 2-4. Experimental apparatus for the continuous wear test.

2.3. Tool and sheet materials

The material used for this study is a 1.2 mm uncoated TRIP steel sheet with a tensile strength of 1180 MPa (TRIP1180) manufactured by POSCO Pohang steelworks. The material properties were characterized using uniaxial tension tests in accordance with the ASTM E8 standard. The measurement was performed using an MTS810 universal testing machine (MTS Systems Corporation, USA). On the sub-size specimen, a constant velocity of 0.025 mm/s

was imposed. Using the ARAMIS DIC system (GOM, Germany), the strain was calculated. Table 2-1 summarizes the uniaxial tensile properties. The insert-type punch was manufactured using POSCO Pohang steelworks' Steel Tool Die (STD)-11 and BÖHLER's K340 tool steels. At a normal load of 0.1 kgf, the Vickers hardness of STD-11 and K340 tool steels were 788.5 ± 12.2 and 831.3 ± 14.4 $HV_{0.1}$, respectively. TRIP1180 steel sheet has a Vickers hardness of 373.2 ± 7.1 $HV_{0.1}$. Table 2-2 contains the chemical compositions of TRIP1180 steel sheet, STD-11, and K340 tool steels. Physical vapor deposition (PVD) was used to deposit CrN and AlTiCrN onto the insert-type punch. As illustrated in Fig. 2-5, an optical microscope was used to determine the thickness of the CrN and AlTiCrN coating layers on the punch radius; the thicknesses obtained were 13.4 ± 0.4 and 14.8 ± 0.9 μm, respectively. Because of the coating layers, a normal load of 0.08 kgf is appropriate for measuring the Vickers hardness of CrN and AlTiCrN coatings, which can ignore the effect of the tool material's hardness. CrN and AlTiCrN coatings have Vickers hardness values of 2,105.9 ± 15.5 and 3,818.3 ± 36.5 $HV_{0.08}$, respectively.

Table 2-1. Mechanical properties of TRIP1180 steel sheet obtained using the uniaxial tensile test.

Thickness (mm)		1.2
Yield stress (MPa)		933
Ultimate tensile stress (MPa)		1196
Swift hardening law $\sigma=k(\varepsilon_0+\varepsilon)^n$	K (MPa)	1584.6
	ε_0	0.0036
	ε	0.0858
R-value	0°	0.7382
	45°	0.9786
	90°	0.8671

Table 2-2. Chemical compositions of TRIP1180 steel sheet and STD-11 and K340 tool steels (wt%).

	TRIP1180	STD-11	K340
C	0.285	1.55	1.10
Si	1.61	0.26	0.90
Mn	2.15	0.30	0.40
Cr	-	11.36	8.30
Mo	-	0.81	2.10
V	-	0.20	0.50
P	0.018	-	-
S	0.001	-	-

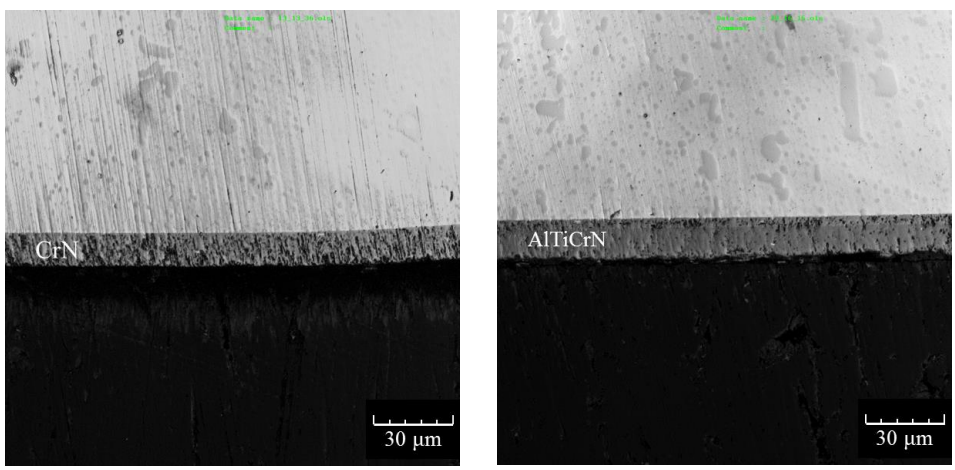

(a) (b)

Fig. 2-5. Thickness of the coating layers. (a) PVD CrN coating, (b) PVD AlTiCrN coating

2.4. Test conditions

To demonstrate the dependence of wear rate sensitivity on the radius of the tool curvature, two punch shapes with a curvature radius of 3.0 mm and 5.5 mm were used to manufacture the punches. Additionally, the wear resistances of STD-11 and K340 tool steels were compared. To determine the effect of coating conditions on wear resistance, we also evaluated the CrN and AlTiCrN coatings deposited using the PVD method. The tooling conditions for the punches used in the wear test are listed in Table 2-3. The continuous wear test was conducted on four different types of punches with varying punch shapes, tool steels, and coating conditions. The punches were subjected to wear tests concurrently because the progressive die set was designed to evaluate the wear characteristics of four different types of punches in a single press stroke. The process and geometric parameters of the continuous wear test are summarized in Table 2-4. A 120 mm wide sheet metal strip is punched, resulting in a blank with a width and length of 20 and 57.5 mm, respectively. To prevent ironing, the die-to-punch gap was applied with a 10% clearance, which is a common practice in the stamping process. The punch stroke for a single stamping stroke was designed to be 35.0 mm. The automatic feeding system feeds the sheet metal into the progressive die set in sections of 75 mm. The press speed was set to 15 strokes per minute (spm), which is the standard

for stamping automotive body parts. A coil spring with a spring constant of 2.02 N/mm was used to apply the padding force. The padding force applied to the sheet metal during stamping is 70.7 N, which is sufficient to hold the blank in place during the process.

Table 2-3. Tool conditions of the punches used in the wear test.

Punch number	Punch shape	Punch material	Coating
1	R3.0	STD-11	PVD CrN
2	R5.5	STD-11	PVD CrN
3	R3.0	K340	PVD CrN
4	R3.0	STD-11	PVD AlTiCrN

Table 2-4. Summary of the process and geometric parameters of the continuous wear test.

Sheet metal width (mm)	120
Pitch (mm)	75
Piercing hole diameter (mm)	4
Blank thickness (mm)	1.2
Blank width (mm)	20
Blank length (mm)	57.5
Die-to-punch gap (mm)	1.32 (10% clearance)
Punch radius (mm)	3.0, 5.5
Punch stroke (mm)	35
Press rate (spm, strokes per minute)	15

2.5. Wear measurement methods

2.5.1. Punch surface profile

Wear is defined as the gradual deterioration and removal of material caused by the relative motion of adjacent working parts [44]. Tool material removal during the stamping process alters the profile of the tool surface. As a result, the punch surface wear depth was quantitatively analyzed to ascertain evolutionary wear behavior. To confirm the punch's initial condition, the surface profile was measured prior to the wear test. The evolutionary wear

characteristics of the punches were determined by measuring the wear characteristics at regular stamping hit intervals. The wear depth of the punch's surface were examined every 5,000 to 10,000 strokes. Wear tests were conducted on the stamped product surface until severe wear tracks were discovered.

The profile of the punch surface was determined using a Leitz Infinity 12.10.6 coordinate measuring machine manufactured by Hexagon AB. It is a contact-type 3-dimensional (3D) coordinate measuring machine with a precision of 0.3 + L/1000 μm (L in mm). To compare the surface profiles in the same region before and after the wear test, it is necessary to understand the reference coordinates of the punch surface. Because the wear in this punch was designed to occur in the curvature center, the reference coordinates were determined from the regions with less possibility for tool wear, which are back, side, and bottom of the punch without contact with the blank. The reference coordinates were measured in the same regions of the punch. By recognizing the reference coordinates, we were able to generate the origin coordinates, which do not change during the wear test. The punch surface profile was determined using these origin coordinates by measuring the region where intense wear was expected to occur owing to the contact with the sheet metal during the stamping process, as indicated in Figure 2-6. By

measuring the punch surface, point data along the measurement line were identified. To achieve surface profile connectivity, the spline option in AUTOCAD2020 was used to connect the points, as shown in Figure 2-6. The wear depth on the punch surface was determined by measuring the distance between the as-produced and post-wear surface profiles along the measuring direction from 55° to 90° on the punch radius.

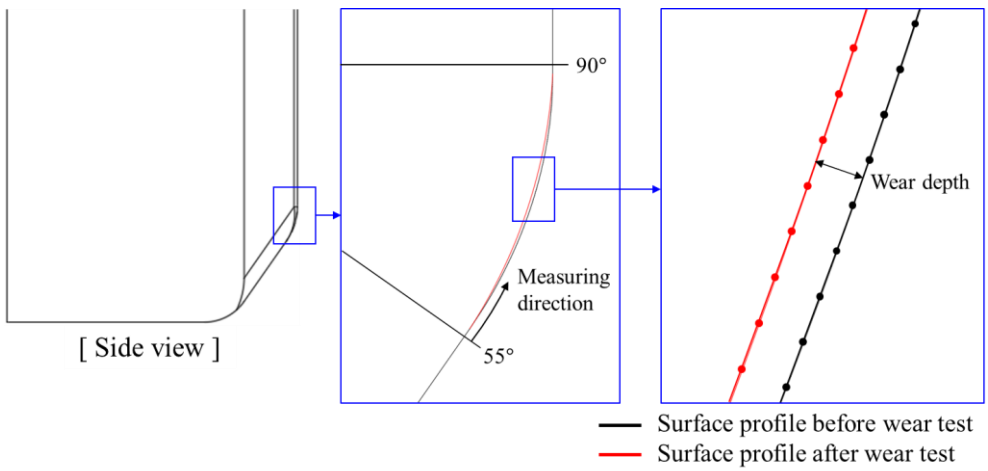

Fig. 2-6. Schematics of measurement method for finding wear depth in terms of the difference in surface profile before and after the wear test.

2.5.2. Punch roughness

Confocal laser scanning microscopy (CLSM; LEXT OLS3100 manufactured by OLYMPUS) was used to determine the roughness of the punch surface. CLSM is a laser-based optical imaging technique. Successive

2D image slices at various depths were captured and merged to reconstruct 3D structures. This property enables 3D imaging and surface profiling of the samples using the CLSM. To ensure an accurate roughness measurement, a 50x objective lens was used for the assessments. The cut-off wavelength was set to 1/3 to eliminate the wave component. The measurement area on the punch radius ranged from 76° to 90°, referring to the area of wear. As shown in Fig. 2-7(a), a punch insert holder device was used to incline the measurement area by 5 degrees to make the measurement area horizontal, which is to improve the accuracy roughness measurement. The individual images were stitched together to create a full view from 76° to 90° on the punch radius. Fig. 2-7(b) shows the desired area to measure the roughness corresponding to each angle on punch surface. The same areas of the punch radius were examined before and after the wear tests to compare the surface conditions. The arithmetical mean height of a surface (Sa) was used to determine the roughness of the surface. Sa is the average of the absolute values of the measured point heights within the desired area, as follows:

$$Sa = \frac{1}{A}\iint_{A} |Z(x,y)|dxdy \tag{3.1}$$

Here, A is the defined area and x and y indicate the coordinates. Z is the height of the measured points within the defined area. Due to the difficulty of

inspecting the surface condition of the punch on a frequent basis, the imaging and roughness of the punch's surface were examined every 5,000 to 10,000 strokes.

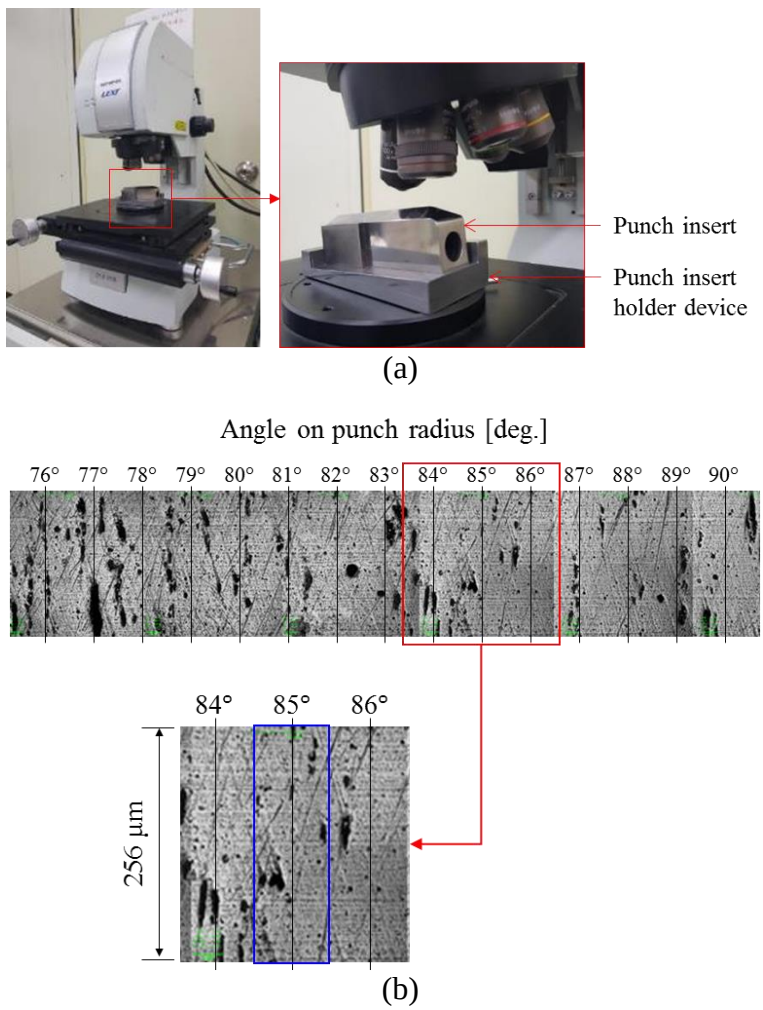

Fig. 2-7. Measuring methods for the punch roughness. (a) a punch insert holder device to incline the measurement area by 5 degrees, (b) desired area to measure the roughness corresponding to each angle on punch radius

2.5.3. Product roughness

CLSM was also used to determine the roughness of the product surface. The surface roughness was measured to up to 30 mm at 5 mm intervals from the line below the formed products, as shown in Fig. 2-8. For the accurate surface roughness measurement, a lens with 50x magnification and cut-off wavelength 1/3 were used. The Sa (Eq. 3.1) was used to determine the roughness of the surface. The roughness of the formed product was measured every 500 strokes.

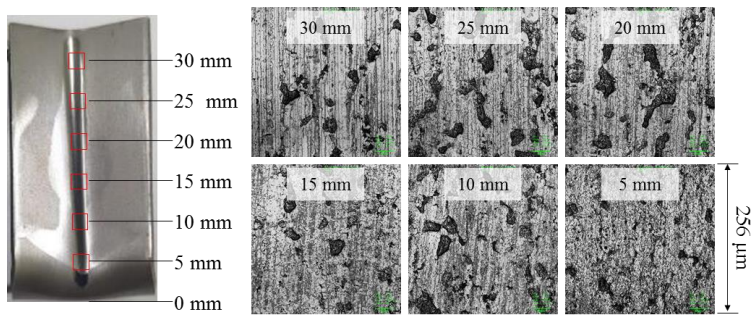

Fig. 2-7. Measuring methods for the formed product roughness.

3. Wear test results

Wear tests were conducted until severe scratches were discovered on the stamped product surface. Fig. 3-1 illustrates the surface conditions of punches and stamped products following wear tests. Punch 1, Punch 2, Punch 3, and Punch 4 were each performed with a maximum of 16,500, 18,000, 25,500, and 59,000 stamping hits, respectively. Prior to the formation of severe scratches on the surface of the product, a scar was observed during the stamping process, but the surface was not rough and demonstrated good quality. After the wear test, the surface of punches and stamped products developed severe wear and rough scratches. Fig. 3-1(a) illustrates the surface conditions of the punch and stamped product following the wear test of Punch 1 (R3.0, STD-11, CrN coating). After 16,000 hits, a scar is found in the regions of the stamped product surface in contact with the punch, but the surface is still even and of good quality. However, after 16,500 hits, the punch surface became severely worn, resulting in rough scratches on the stamped product surface. Fig. 3-1(b) shows the wear test results of Punch 2 (R5.5, STD-11, CrN coating). Due to the 5.5 mm punch radius, a relatively wide scar appears on the stamped product surface. After 17,500 punches, the stamped product regions in contact with the punch are even and clear. However, after

18,000 hits, severe defects are discovered on the surfaces of punch and stamped products. Comparing Punch 1 and Punch 2, which are made of STD-11 tool steel and coated with CrN, Punch 2 with a curvature radius of 5.5 mm outperforms Punch 1 with a radius of 3.0 mm in terms of wear resistance, as the smaller curvature radius experiences more contact pressure. As illustrated in Fig. 3-1(c), a scar is visible in the regions of the stamped product surface in contact with of Punch 3 (R3.0, K340, CrN coating) after 25,000 hits. However, severe defects on the surface of a stamped product and punch occur after 25,500 hits. The tool material also play a significant role in the wear resistance. When comparing the wear resistance of Punch 1 and Punch 3, both of which are coated with the same CrN and manufactured in the same shape of R3.0, Punch 3 made of K340 tool steel outperforms Punch 1 made of STD-11 tool steel, because the hardness of K340 ($831.3 \pm 14.4\ HV_{0.1}$) is greater than that of STD-11 ($788.5 \pm 12.2\ HV_{0.1}$). Fig. 3-1(d) illustrates the surface conditions of the punch and stamped product following the wear test of Punch 4 (R3.0, K340, AlTiCrN coating). After 58,500 hits, the stamped product's regions in contact with Punch 4 exhibit excellent surface quality. However, after 59,000 hits, severe defects were discovered on the surface of the punch and stamped product. Surface coatings are critical for increasing the wear resistance of stamping tools. When Punch 1 and Punch 4 have the same

curvature radius of 3.0 mm and are made of the same STD-11 tool steel, Punch 4 coated with AlTiCrN showed superior wear resistance than Punch 1 coated with CrN, because AlTiCrN has a hardness of 3,818.3 ± 36.5 $HV_{0.08}$, which is greater than the hardness of CrN, 2,105.9 ± 15.5 $HV_{0.08}$. Punches with small curvature radius wear rapidly, while tools and coatings with a high hardness have high resistance against wearing. Thus, the proposed testing method can be used to obtain reliable results for quantitatively and qualitatively evaluating the wear lifetime of various tooling and process parameters.

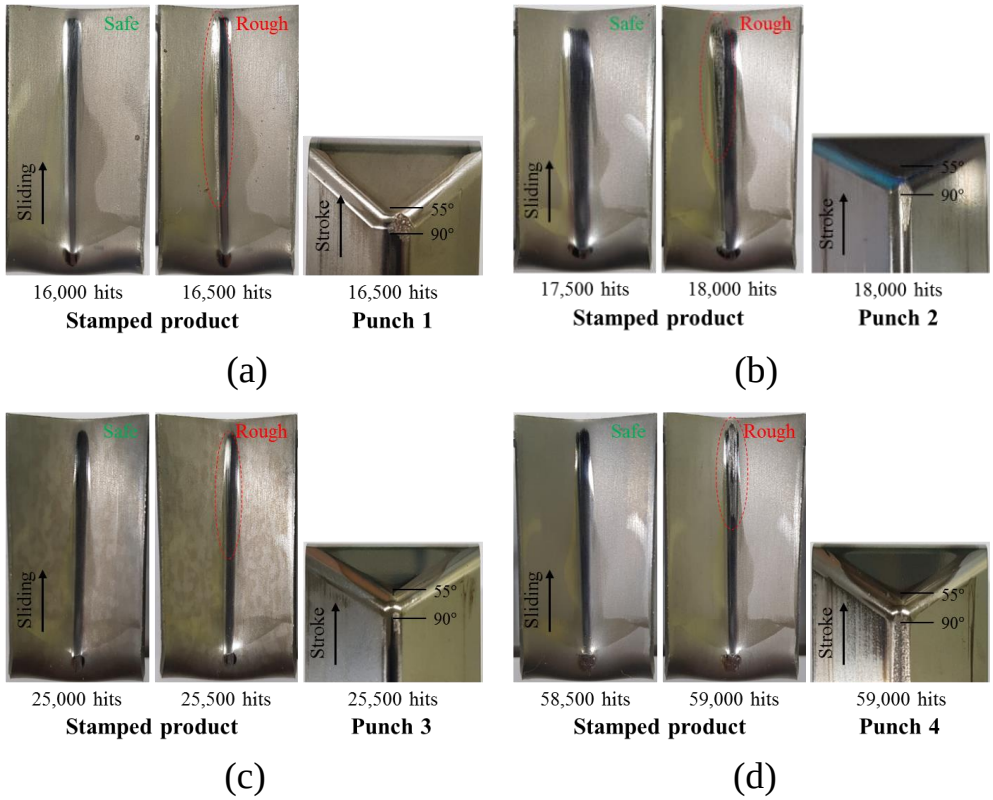

Fig. 3-1. Surface conditions of the punches and stamped products after wear tests. (a) Punch 1 (R3.0, STD-11, CrN coating), (b) Punch 2 (R5.5, STD-11, CrN coating), (c) Punch 3 (R3.0, K340, CrN coating), (d) Punch 4 (R3.0, STD-11, AlTiCrN coating)

3.1. Wear depth

Fig. 3-2 illustrates the wear depth results for each punch. For all punches, the wear depths were very small and close to 0, and the deviations were within the measurement error before severe scratches occur on the stamped products. However, the wear depth of the punches increases significantly when severe

scratches occur on the stamped products. Punch 1 wore from 81° to 90° on the punch radius after 16,500 stamping hits, as illustrated in Fig. 3-2(a). Punch 1 has a maximum wear depth of 8.6 μm at an angle of 88° on the punch radius, which is less than the CrN coating thickness of 13.4 ± 0.4 μm. After 18,000 stamping hits on Punch 2, wear occurred in a relatively wide range of about 80° to 90° on the punch radius, as illustrated in Fig. 3-2(b). Punch 2 has a maximum wear depth of 15.7 μm at an angle of 87° on the punch radius. Because the CrN coating thickness is 13.4 ± 0.4 μm, it is confirmed that the CrN coating is completely peeled off. After 25,500 hits on Punch 3, wear occurred between 84° and 90° on the punch radius, as illustrated in Fig. 3-2(c). Punch 3 has a shallow wear depth, with a maximum wear depth of 8.7 μm at an angle of 85° on the punch radius, which is less than the CrN coating thickness of 13.4 ± 0.4 μm. After 59,000 stamping hits on Punch 4, wear occurred between 84° and 90° on the punch radius, as illustrated in Fig. 3-2(d). Punch 4 has a maximum wear depth of 17.4 μm at an angle of 87° on the punch radius. Because the AlTiCrN coating thickness is 14.8 ± 0.9 μm, the AlTiCrN coating is completely peeled off. The wear area of all punches were confirmed to be in contact with the sheet metal from approximately 80° to 90° on the punch radius. All tests are successful in determining the wear characteristics and behavior of all punches, and we found that the wear occurs

between approximately 80° and 90° on the punch radius and wear depth increases rapidly following the failure.

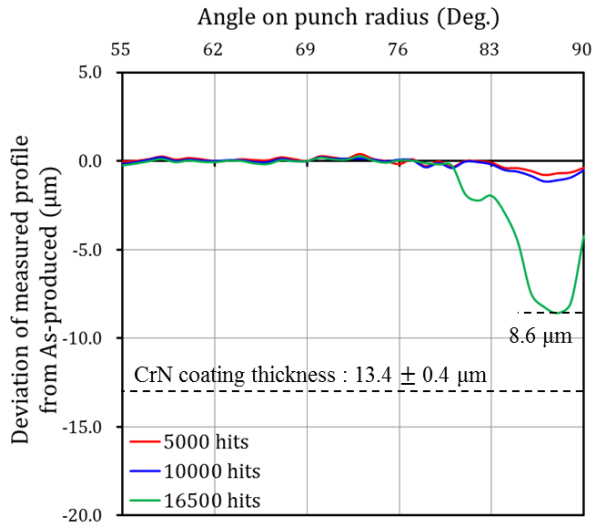

(a)

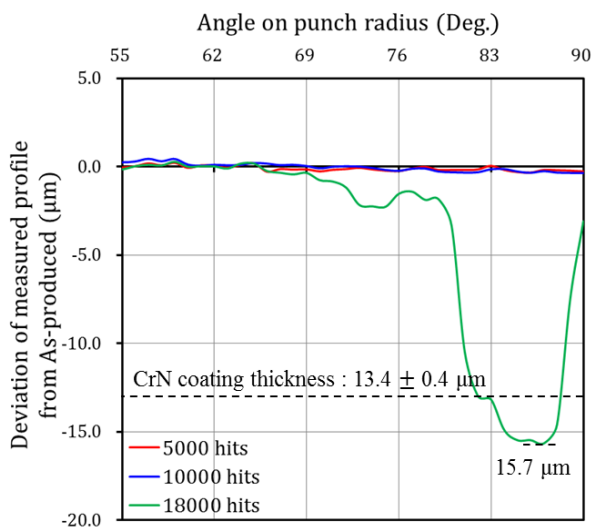

(b)

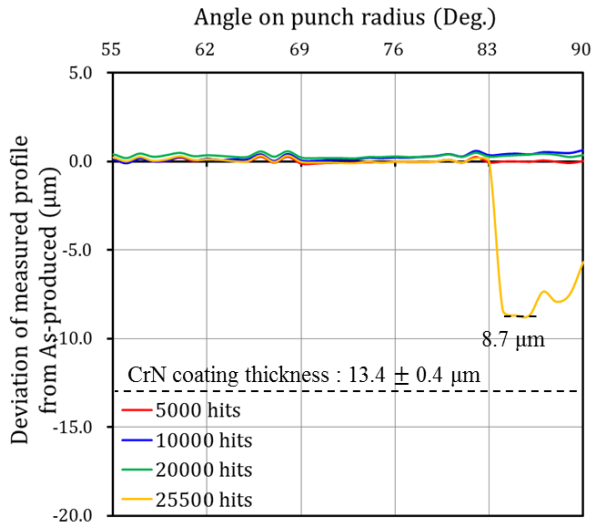

(c)

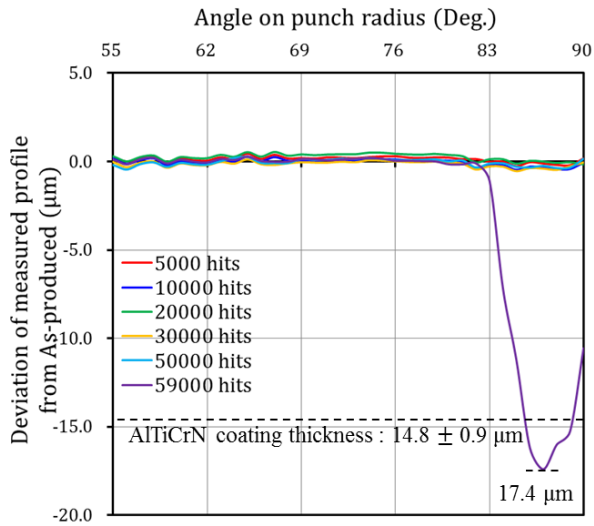

(d)

Fig. 3-2. Wear depth for each punch. (a) Punch 1 (R3.0, STD-11, CrN coating), (b) Punch 2 (R5.5, STD-11, CrN coating), (c) Punch 3 (R3.0, K340, CrN coating), (d) Punch 4 (R3.0, STD-11, AlTiCrN coating)

3.2. Punch roughness

The surface imaging and roughness for all punches in relation to stamping hits were inspected to determine the surface condition of the punch until it failed. Due to the difficulty of inspecting the surface condition of the punch on a frequent basis, the imaging and roughness of the punch's surface were examined every 5,000, 10,000, and 20,000 strokes.

Fig. 3-3 shows the surface imaging and measured roughness of Punch 1 in relation to stamping hits. The imaging and roughness of the punch's surface were examined prior to the wear test (as-produced), and at 5,000, and 10,000 hits, as well as after failure (16,500 hits). The image of the punch surface are illustrated in Fig. 3-3(a) to compare the surface conditions before and after the wear tests. Fig. 3-3(b) shows the results of the measured punch roughness before and after the wear test. Before the wear test, the roughness of as-produced did not exceed 0.3 μm, and the average roughness was about 0.2 μm. After the wear test of 5,000 and 10,000 hits, the micro-scratches were found in the sliding direction in the surface image, and a dark scar was visible on the punch radius between 83° and 85°. Moreover, the measured roughness was approximately 0.1 μm higher than that of as-produced over the entire measurement area, and the roughness measured on the punch radius between

83° and 85° was approximately 0.5 μm. However, after the wear test of 16,500 hits, the surface roughness over the entire area on the punch radius increased sharply, and it had a maximum value of 1.812 μm at 86°.

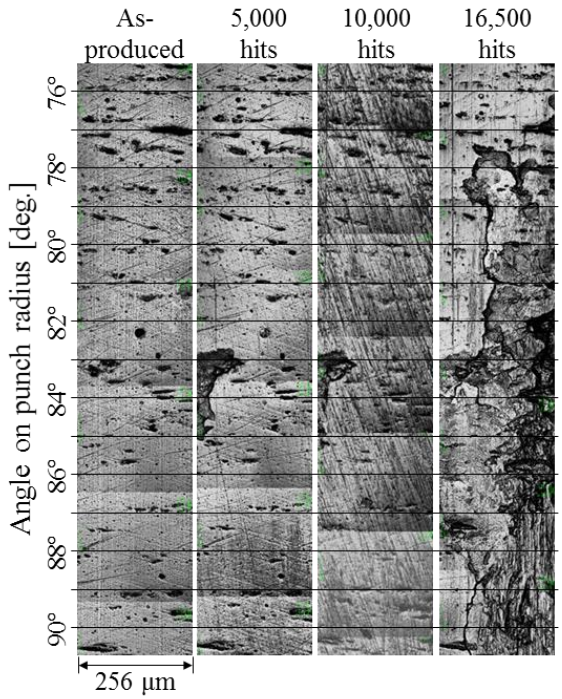

(a)

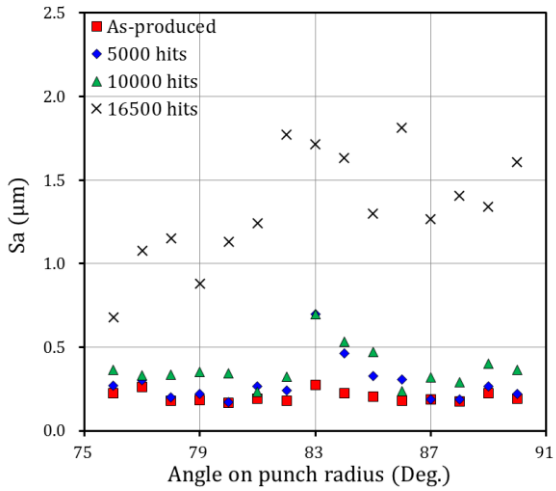

(b)

Fig. 3-3. The surface condition of Punch 1 (R3.0, STD-11, CrN coating) before and after the wear test. (a) surface imaging, (b) surface roughness

As illustrated in Fig. 3-4, the surface imaging and roughness of Punch 2 in relation to stamping hits were inspected to determine the surface condition of the punch until it failed. The roughness of as-produced did not exceed 0.3 μm, and the average roughness was about 0.23 μm. After the wear test of 5,000 and 10,000 hits, the roughness measured showed no significant difference from that of as-produced, but the micro-scratches were found over the entire measurement area in the sliding direction. However, after the wear test of 18,000 hits, the surface roughness over the entire measurement area increased noticeably, and it had a maximum value of 1.668 μm at 82°.

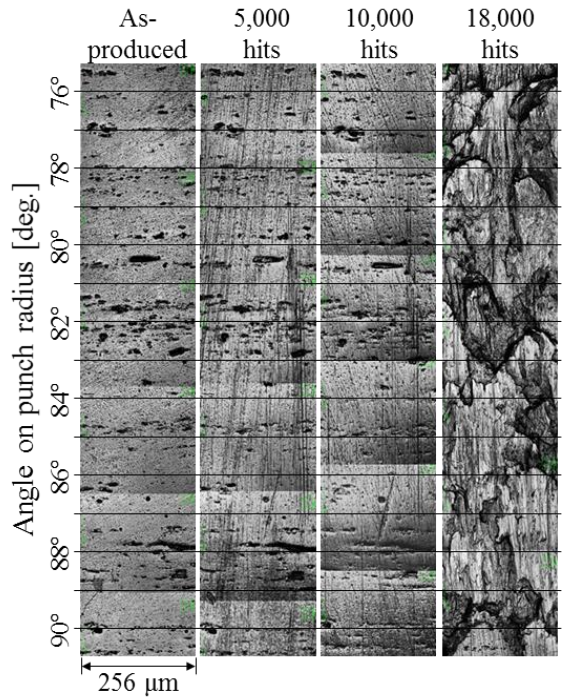

(a)

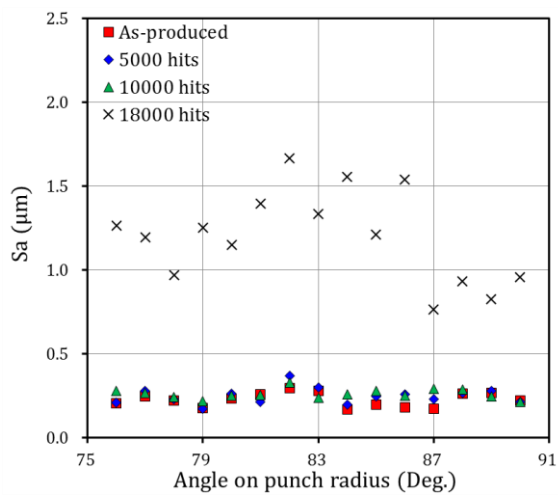

(b)

Fig. 3-4. The surface condition of Punch 2 (R5.5, STD-11, CrN coating) before and after the wear test. (a) surface imaging, (b) surface roughness

Fig. 3-5 shows the surface imaging and measured roughness of Punch 3 in relation to stamping hits. The imaging and roughness of the punch's surface were examined for as-produced, and at 5,000, 10,000, and 20,000 hits as well as after failure (25,500 hits). Fig. 3-5(a) illustrates the image of the punch surface. The results of the measured punch roughness are shown in Fig. 3-5(b). The as-produced exhibit excellent surface quality with no defects. The surface roughness of as-produced were less than 0.40 μm, with an average roughness of approximately 0.25 μm. Although the micro-scratches were found on the punch radius after the wear test of 5,000, 10,000, and 20,000 hits, the roughness measured was comparable to that of As-produced. However, after the wear test of 25,500 hits, the severe wear was found from 84° to 90° on the punch radius, and the surface roughness measured had values of approximately 0.5 μm to 1.0 μm.

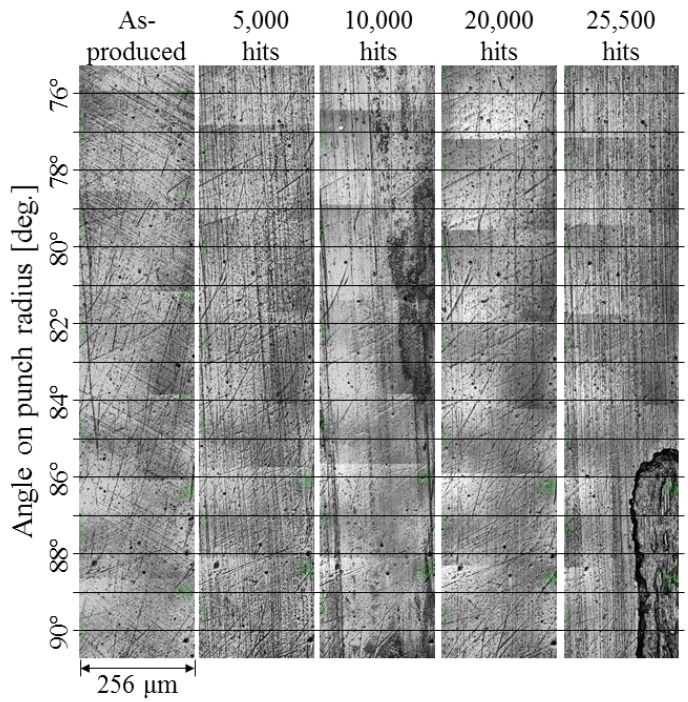

(a)

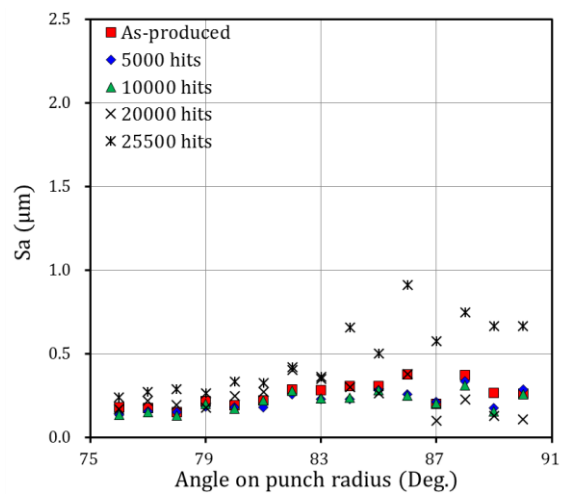

(b)

Fig. 3-5. The surface condition of Punch 3 (R3.0, K340, CrN coating) before and after the wear test. (a) surface imaging, (b) surface roughness

As illustrated in Fig. 3-6, the surface imaging and roughness of Punch 4 in relation to stamping hits were inspected to determine the surface condition of the punch until it failed. Due to the difficulty of inspecting the surface condition of the punch on a frequent basis, the imaging and roughness of the punch's surface were examined prior to the wear test (as-produced), and at 5,000, 10,000, 20,000, 30,000, and 50,000 hits, as well as after failure (59,000 hits). The image of the punch surface and the desired area where the roughness corresponding to each angle was measured are shown in Fig. 3-6(a). The results of the measured punch roughness before and after the wear test are shown in Fig. 3-6(b). The as-produced exhibit excellent surface quality with no defects or scratches. The surface roughness of as-produced were less than 0.30 μm, with an average roughness of approximately 0.23 μm. Moreover, a dark scar is visible on the punch radius between 87° and 89°. Because severe scratches on the stamped product surface occurred after 59,000 hits and the wear depth of the punch surface measured up to 50,000 hits is close to 0 (see Fig. 3-2(d)], the dark scar extending from 87° to 89° on the punch radius is surface contamination or micro surface defects. After 10,000 hits, there were no scratches on the punch surface, and the measured surface roughness is comparable to that of as-produced. After 20,000 hits, micro-scratches appear in all measurement areas along the stroke direction.

Micro-scratches, on the other hand, had no effect on the increase in roughness. Punch surface images taken after 30,000 and 50,000 hits show an increase in scratches in the sliding direction, resulting in an increase in surface roughness of approximately 0.15 μm from 82° to 87° on the punch radius. After 59,000 hits, a severe wear track was discovered on the punch radius between 78° and 90°, which is consistent with the wear depth results for Punch 4 (see Fig. 3-2(d)). However, the worn area has a surface roughness of approximately 1.0 μm, which is significantly greater than the unworn area itself. As previously stated, wear occurs between approximately 80° and 90° on the punch radius for all punches. Thus, a slight increase in roughness prior to failure is assumed to result in severe wear, and the area of these scratches is considered an initiation site for severe wear.

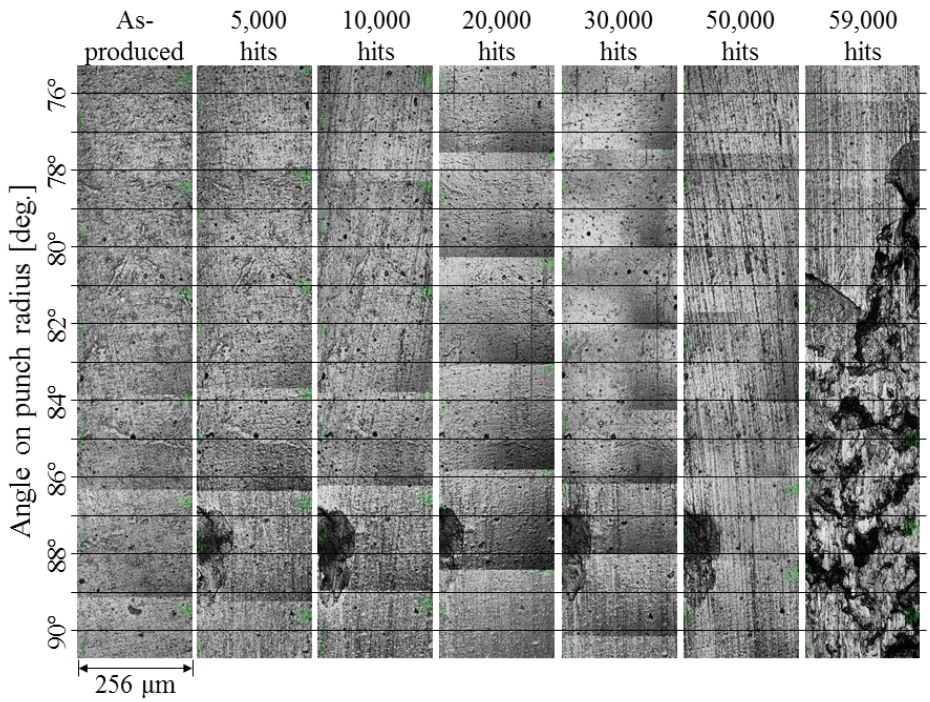

(a)

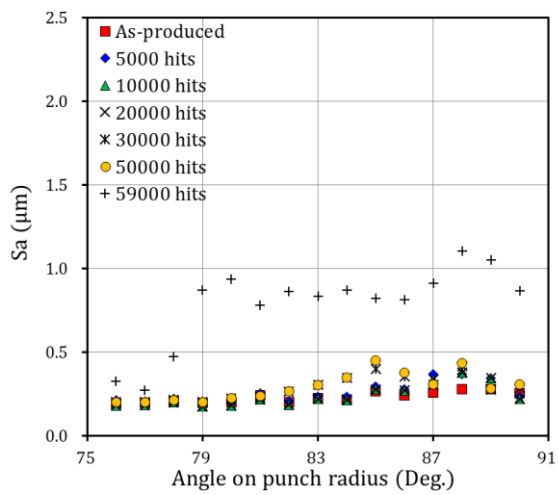

(b)

Fig. 3-6. The surface condition of Punch 4 (R3.0, K340, AlTiCrN coating) before and after the wear test. (a) surface imaging, (b) surface roughness

3.3. Product roughness

Fig. 3-7 shows the product roughness at each measuring area. The roughness of the products formed before the failure was approximately constant at each measuring area, which is similar to 0.582±0.018 μm (roughness of As-received). During the stamping process, the specimen comes into contact with the punch and then 5 mm measurement area of the specimen is bent first. As the punch stroke progresses, the punch slides in the direction of 30 mm measurement area of the specimen. Therefore, relatively high roughness was measured at 5 mm measurement area from the line below the formed products, and the roughness measured gradually decreased toward 30 mm measurement area. For the roughness of the product formed with Punch 1 (see Fig. 3-7(a)), the roughness measured had relatively high values of approximately 1.0 μm after the wear test of 16,500 hits, which is found at 20 mm to 30 mm measurement area. Fig. 3-7(b) shows the roughness of the product formed with Punch 2. Very high values of the roughness were measured at 10 mm to 30 mm measurement area after 18,000 hits, and a maximum roughness of 2.43 μm was measured at 30 mm measurement area. Fig. 3-7(c) shows the roughness of the product formed with Punch 3. Relatively high values of roughness above 1.0 μm were measured at 25 mm, 30 mm after the wear test of 25,500 hits. For the roughness of the product

formed with Punch 4 (see Fig. 3-7(d)), the roughness measured had relatively very high values after the wear test of 59,000 hits, which is found at 25 mm, and 30 mm measurement area. During the stamping process, the specimen first comes into contact with the punch radius of 55°. As the punch stroke progresses, the contact between the specimen and tool proceeds to tool radius of 90°. Therefore, the worn area of the punch, punch radius from 80° to 90°, comes into contact with 25 and 30 mm from the product bottom line.

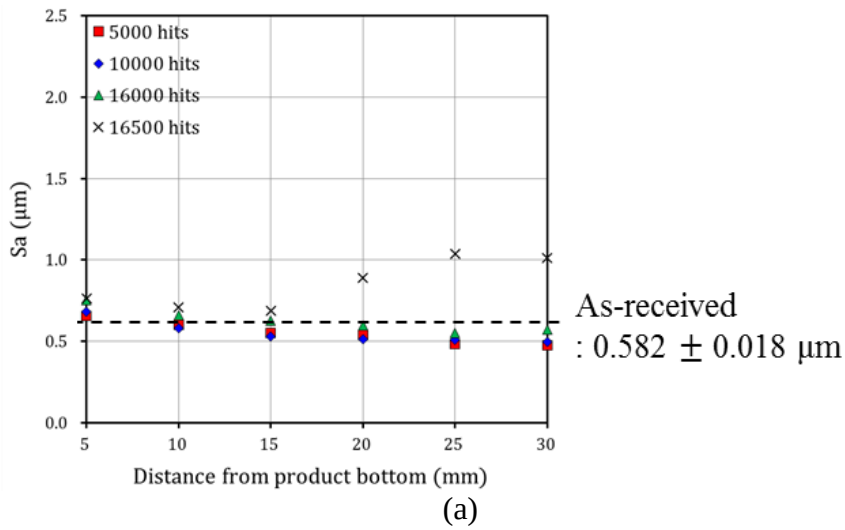

(a)

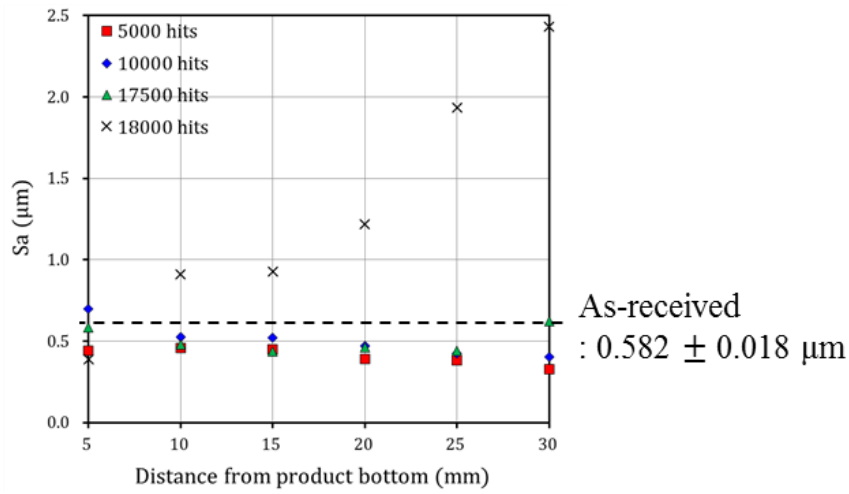
5000 hits
10000 hits
17500 hits
18000 hits
Sa (μm)
Distance from product bottom (mm)
As-received
: 0.582 ± 0.018 μm

(b)

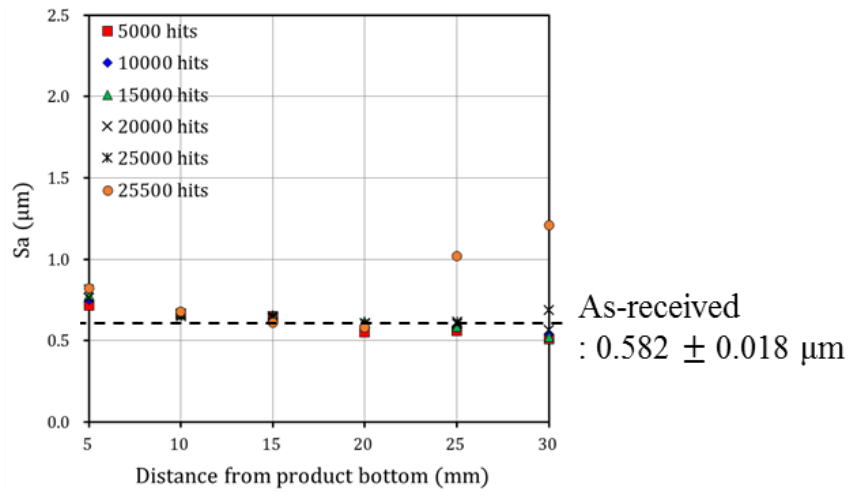
5000 hits
10000 hits
15000 hits
20000 hits
25000 hits
25500 hits
Sa (μm)
Distance from product bottom (mm)
As-received
: 0.582 ± 0.018 μm

(c)

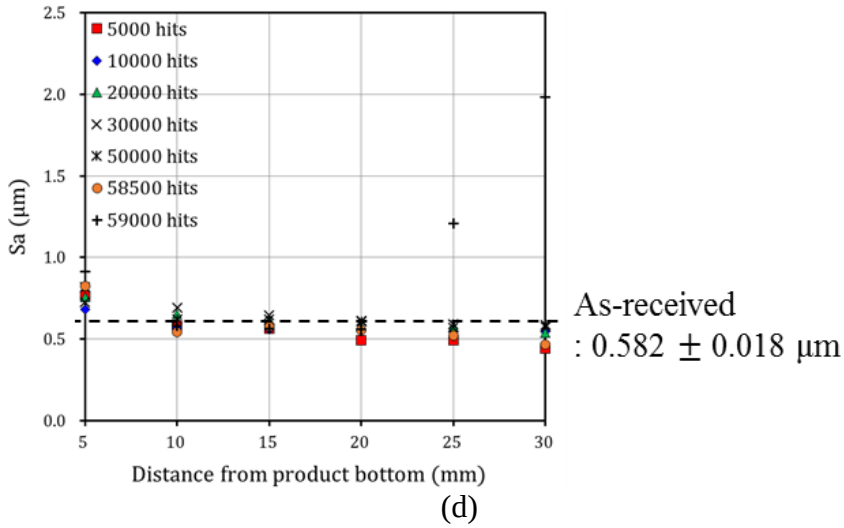

Fig. 3-7. The product roughness measured. (a) the roughness of the product formed with Punch 1, (b) the roughness of the product formed with Punch 2, (c) the roughness of the product formed with Punch 3, (d) the roughness of the product formed with Punch 4

3.4. Discussion

The purpose of this study is to detail a novel method for testing and evaluating the wearing of tools used in the sheet metal forming process. The disadvantage of conventional wear testing apparatus is that it requires placing the sheet metal on the stamping tool and removing it after the stamping process, which is inefficient and time-consuming when performing wear tests with several stamping hits. To address these shortcomings, a systematic wear test process based on the progressive die is proposed, which is capable of evaluating the wear characteristics of four different types of punches simultaneously. Additionally, because a rolled steel coil was used directly for the continuous wear test, this method conserves raw materials and eliminates the need for specimen production. If 10,000 stamping hits are made at a press rate of 15 spm, it will take approximately 11 h to conduct the wear test on four different types of punches concurrently. Thus, the proposed test method can help save time and cost as well as reduce the labor when evaluating the wear lifetime of various tool conditions. Moreover, the punch was made in the form of an insert. As a result, wear tests can be conducted on punches manufactured under a variety of manufacturing conditions, including tool materials, punch shapes, and coating conditions. Additionally, it is designed to replace and examine worn-out punches conveniently and efficiently.

When defects on the punch surface are compared to the condition of a newly manufactured tool, the condition of the punch surface deteriorates. As a result, the surface roughness and surface imaging of the punch radius of Punch 4 were examined in order to confirm the wear track and characterize the wear characteristics and mechanism of wear. As illustrated in Fig. 3-6(a), no adhered or transferred wear fragments were discovered on the punch surface prior to the initiation of severe wear. Additionally, Grooves and ridges parallel to the blank sliding direction were found over entire contact regions on the punch radius and surface roughness increased from 82° to 87° on the punch radius prior to the initiation of severe wear. The micro-scratches generated on the punch surface did not lead to a noticeable change in the surface profile. Therefore, it was confirmed that the micro-scratches prior to failure occurs due to plowing mechanism because the material was not removed from the punch surface and only the micro-scratches are formed during the stamping process [45]. During the continuous stamping of uncoated steel sheets, a repeated tangential load is generated on the friction interface. A noticeable change in the surface profile is not detected prior to failure, but the coating layers of the punches were peeled off following the initiation of severe wear, as illustrated in Fig. 3-6(a). Therefore, fretting wear is considered the wear mechanism of coated tools in stamping of uncoated steel sheets. The fretting

wear is one of the types of fatigue wear, and is caused by a tangential cycling load between two surfaces during friction. The tangential cycling load generates alternating compression-tension stresses, resulting in surface fatigue [46]. Voevodin et al. [47] confirmed that cracks were caused by tangential cycling load during repetitive fretting contact, as shown in Fig. 3-8. Fig. 3-9 shows the evolution of the fretting wear on MoS_2 coating [48]. At 10^5 cycles, some micro-cracks were initiated and propagated due to repeated cyclic tangential load. More micro-cracks were observed at $1.4x10^5$ cycles, and finally the MoS_2 coating was delaminated. Fig. 3-10 shows the fretting surfaces of the fretting wear scar on CrN coating [49]. Fig. 3-10(b) shows the cracks observed at the edge of the fretting wear scar on the CrN coating, which is caused by repeated cyclic tangential load. These cracks join together to form large fretting wear scar, as shown in Fig. 3-10(c−d). To characterize the wear characteristics and mechanism during the stamping of a 1.2-mm-thick uncoated TRIP1180 steel sheet, wear scar on the CrN coating surface of Punch 1 was observed using the CLSM with a 100x objective lens, as shown in Fig. 3-11. In Fig. 3-11(a), the cracks were observed at the edge of the wear scar. Fig. 3-11(b) shows the surface condition in which the CrN coating is peeled off due to the coalescence of the cracks. Therefore, fretting wear is critical to the wear mechanism of coated tools in stamping of uncoated steel

sheets. Measuring the surface roughness, imaging the surface, and examining the wear depth enables effective analysis of the tool wear characteristics and mechanism during the stamping process.

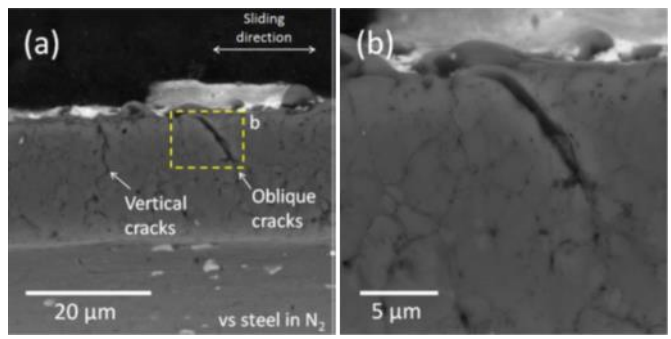

Fig. 3-8. Cross-sectional images of the fretting wear scar on duplex chameleon/PEO coating [47].

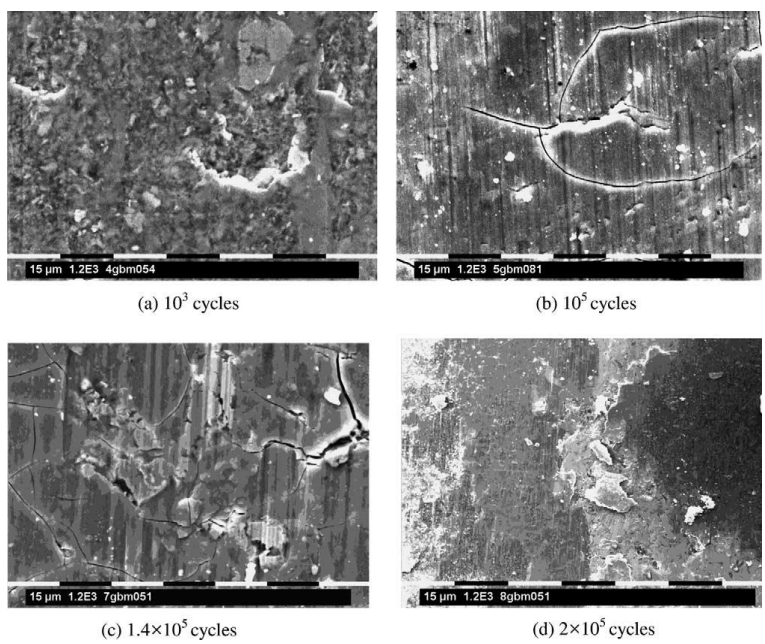

(a) 10^3 cycles (b) 10^5 cycles

(c) 1.4×10^5 cycles (d) 2×10^5 cycles

Fig. 3-9. The evolution of the fretting wear on MoS_2 coating [48].

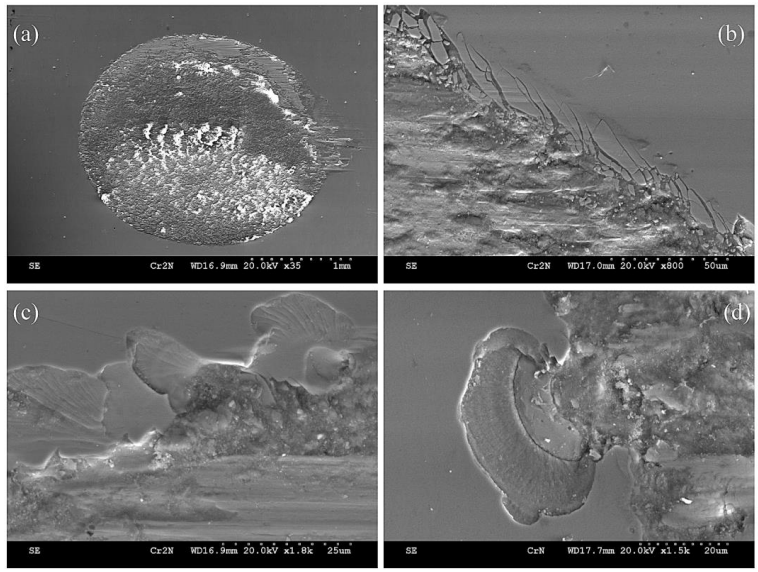

Fig. 3-10. The fretting surfaces of the fretting wear scar on CrN coating [49].

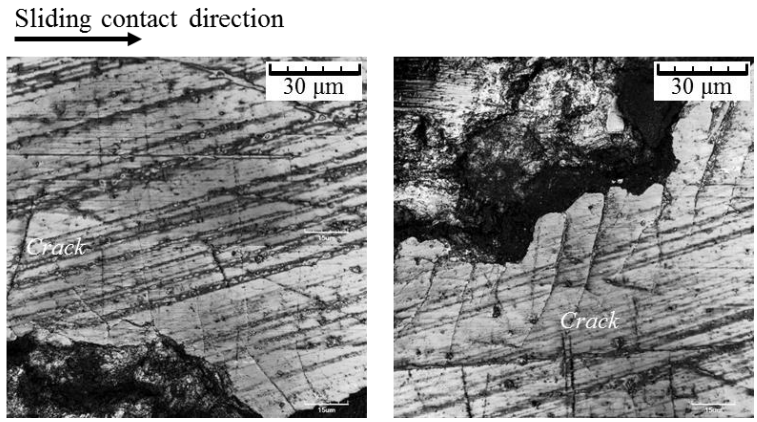

(a)

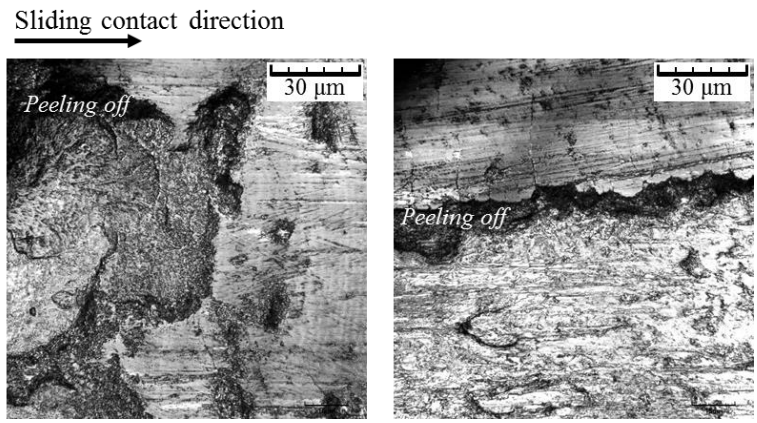

(b)

Fig. 3-11. The wear scar on the CrN coating surface of Punch 1, observed using the CLSM with a 100x objective lens. (a) the cracks at the edge of the wear scar, (b) delamination of CrN coating due to the coalescence of the cracks

Prior to the discovery of severe scratches on the stamped product surface (see Fig. 3-1(d)), no severe defects were discovered on the punch surface (see Fig. 3-5(a)), and the wear depth and roughness of the punch were comparable

to those of the as-produced punch (see Fig. 3-2(d), and Fig. 3-5(b)), as well as the roughness of the formed product was similar to that of the as-received (see Fig. 3-7(d)). However, when severe scratches develop on the stamped product surface after 59,000 stamping hits (see Fig. 3-1(d)), wear begins to appear on the punch surface (see Fig. 3-2(d), and Fig. 3-5). This indicates that the surface condition of the punch has a direct effect on the surface quality of the product.

As illustrated in Fig. 3-12, the surface condition and roughness of stamped products were determined prior to and after failure using the CLSM. For accurate roughness measurement, a 50x objective lens with a cut-off wavelength of 1/3 was used. Prior to the failure, micro scratches in the stamping direction were discovered on all stamped product surfaces, but no critical defects were discovered. The stamping direction is the direction in which the punch contacts and slides across the sheet metal. Roughness was approximately 0.45–0.60 μm. However, the surfaces of all stamped products were extremely rough following failure. As illustrated in Fig. 3-12(a) and (c), severe scratches in the stamping direction were discovered on the product surfaces stamping following failure for Punch 1 and 3, with roughness values of 0.805 and 1.210 μm, respectively. In comparison, as illustrated in Fig. 3-12(b) and (d), the product surface obtained by stamping after failure for Punch

2 and 4 is extremely rough, with no scratches in the stamping direction. The measured roughness of the product is 2.430 and 1.983 μm, respectively, which is significantly greater than the roughness of the product surface stamped with Punch 1 and 3. To confirm the differences in product surface conditions, the CLSM was used to observe the punch surfaces. To capture the magnified images and evaluate the close surface condition, an objective lens with a magnification of 100x was used. As illustrated in Fig. 3-13, the 3D structures of worn punches were observed to confirm the profile and condition of the surface. The worn area of Punch 1 and 3 is relatively smooth, and the depth of wear appears to be less than about 10 μm, as illustrated in Fig. 3-13(a) and (c). Additionally, as illustrated in Fig. 3-2(a) and (c), the wear depth is less than the coating thickness and not all coating layers come off. Because the hardness of the CrN coating (2,105.9 ± 15.5 $HV_{0.08}$) is significantly greater than that of the TRIP1180 steel sheet (373.2 ± 7.1 $HV_{0.1}$), the worn coating layer surface plows the product, resulting in severe scratches in the stamping direction. Otherwise, as illustrated in Fig. 3-13(b) and (d), the worn areas of Punch 2 and 4 are extremely rough. As illustrated in Fig. 3-2(b) and (d), the wear depth of punches 2 and 4 is greater than the coating thickness, indicating that all coating layers have been peeled away. Because the STD-11 tool material, which has a lower hardness than a coating, comes into

contact with the sheet metal, the surface of the stamped product is extremely rough.

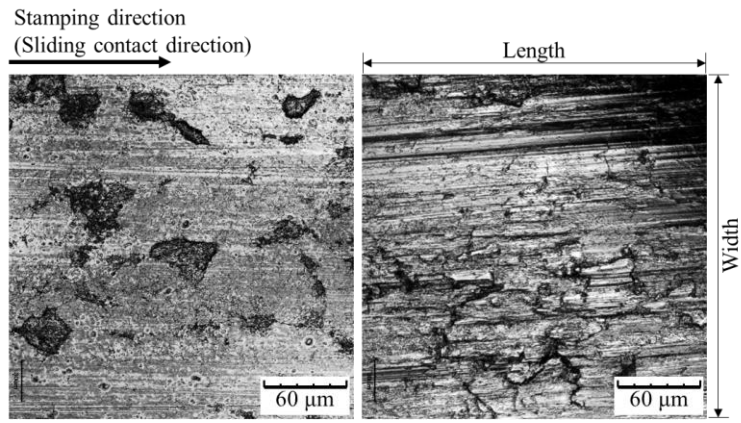

16,000 hits (before failure)
Sa: 0.572 µm

16,500 hits (after failure)
Sa: 0.805 µm

(a)

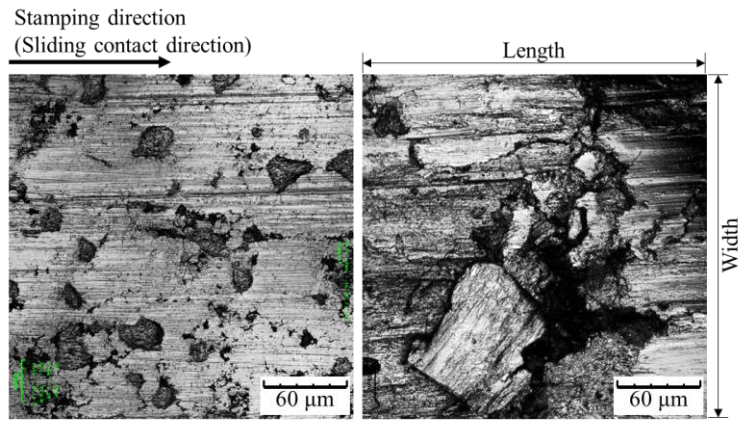

17,500 hits (before failure)
Sa: 0.442 µm

18,000 hits (after failure)
Sa: 2.430 µm

(b)

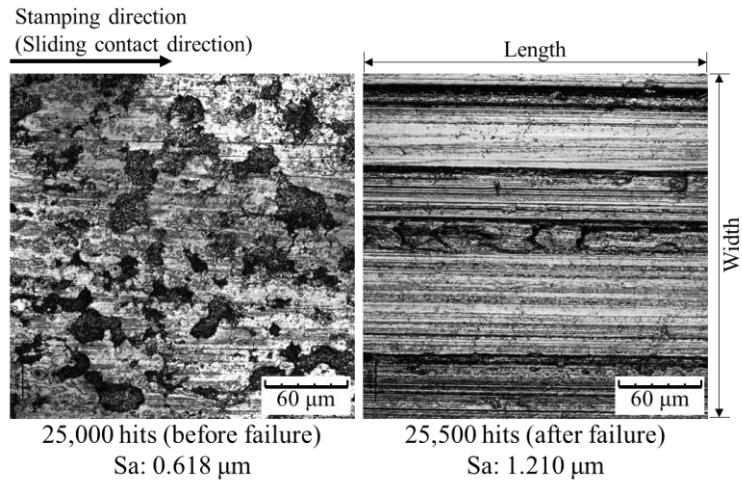

(c)

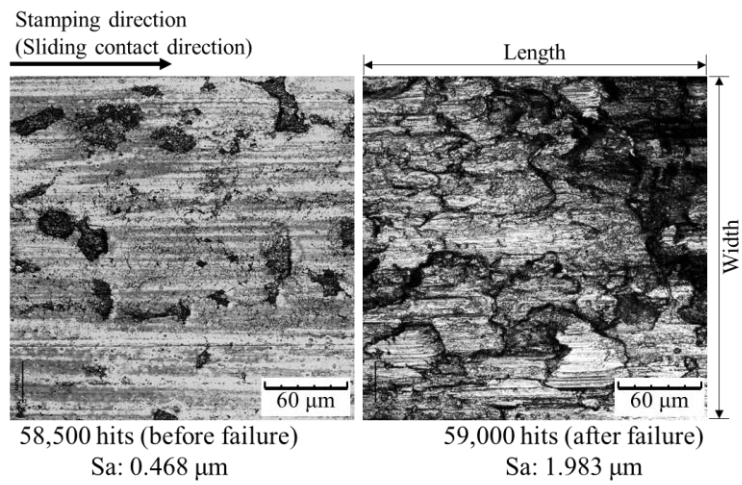

(d)

Fig. 3-12. Surface conditions and roughness of the products before and after failure. (a) Punch 1 (R3.0, STD-11, CrN coating), (b) Punch 2 (R5.5, STD-11, CrN coating), (c) Punch 3 (R3.0, K340, CrN coating), (d) Punch 4 (R3.0, STD-11, AlTiCrN coating)

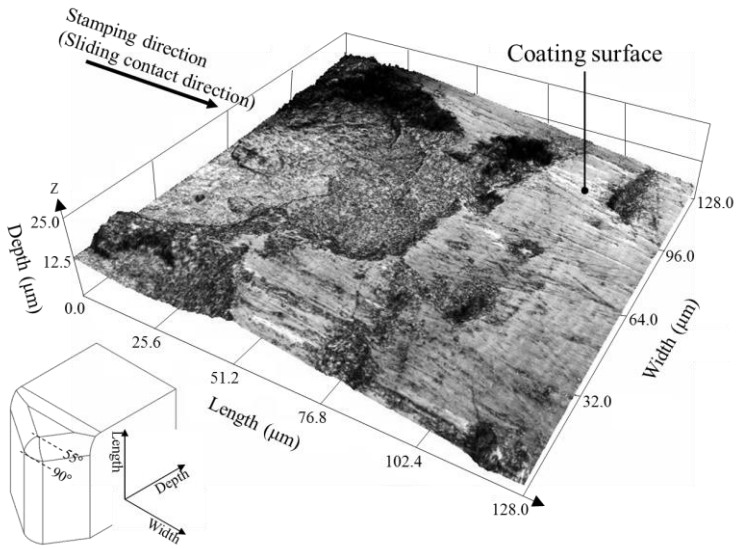
Stamping direction
(Sliding contact direction)
Coating surface
Z
25.0
12.5
0.0
Depth (μm)
25.6
51.2
76.8
102.4
128.0
Length (μm)
128.0
96.0
64.0
32.0
Width (μm)
55°
90°
Length
Depth
Width

(a)

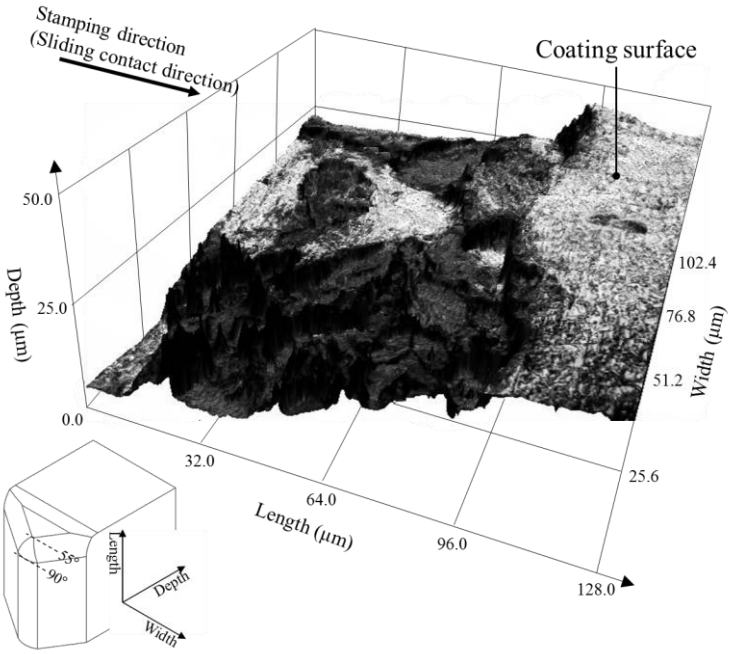
Stamping direction
(Sliding contact direction)
Coating surface
50.0
25.0
0.0
Depth (μm)
32.0
64.0
96.0
128.0
Length (μm)
102.4
76.8
51.2
25.6
Width (μm)
55°
90°
Length
Depth
Width

(b)

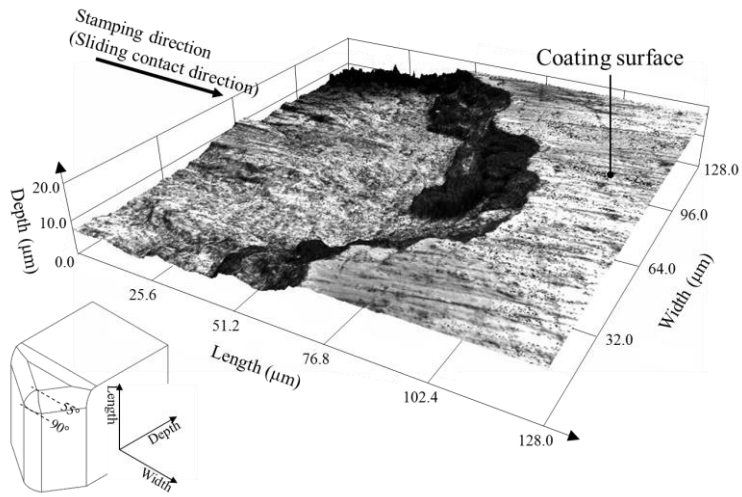

(c)

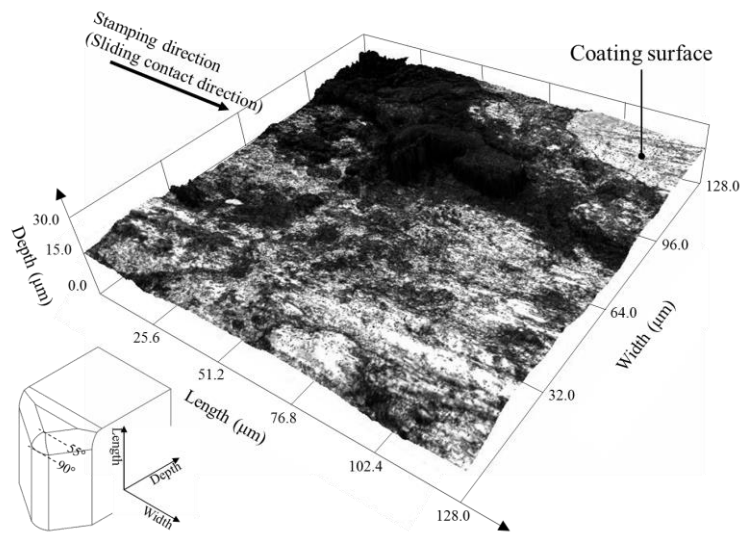

(d)

Fig. 3-13. 3-D structures of the punch worn area. (a) Punch 1 (R3.0, STD-11, CrN coating), (b) Punch 2 (R5.5, STD-11, CrN coating), (c) Punch 3 (R3.0, K340, CrN coating), (d) Punch 4 (R3.0, STD-11, AlTiCrN coating)

All punches were examined for evolutionary wear behavior in relation to stamping hits, as illustrated in Fig. 3-14. In Fig. 3-14, the red and blue marks indicate the wear depth and surface roughness, respectively. The blue rhombus marks indicate the punch roughness, and the blue circle mark indicate the product roughness. Prior to the occurrence of severe defects, the wear depths of all punches were close to 0, the roughness of punches were approximately 0.25 μm, and the roughness of products were approximately 0.55 μm. However, it is observed that for all punches, the wear depth and roughness of the punches and products measured after failure are significantly higher than that measured before failure. It is established that the wear depth behavior in relation to the stamping hits is consistent with the surface roughness of the punches and products and that the measured wear depth accurately represents the wear state. Therefore, the proposed testing method is effective for conducting wear tests on tools manufactured under different conditions and quantitatively evaluating tool wear behavior during the sheet metal forming process. Additionally, using the experimental results obtained from the proposed testing method, it is possible to construct an empirical, reliable wear prediction model.

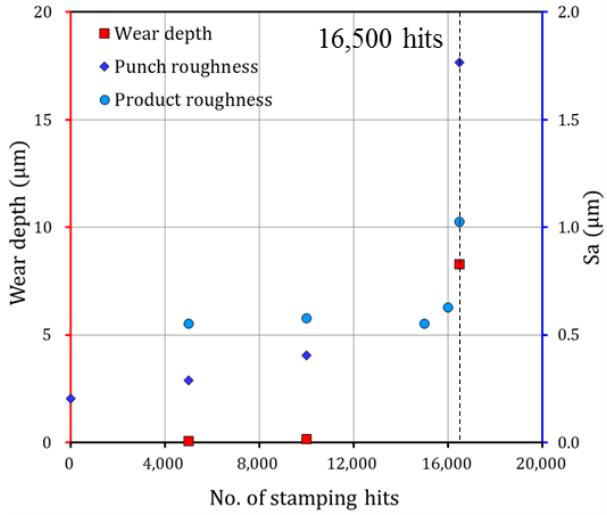
Wear depth
Punch roughness
Product roughness
16,500 hits
Wear depth (µm)
Sa (µm)
No. of stamping hits
0
4,000
8,000
12,000
16,000
20,000
0
5
10
15
20
0.0
0.5
1.0
1.5
2.0

(a)

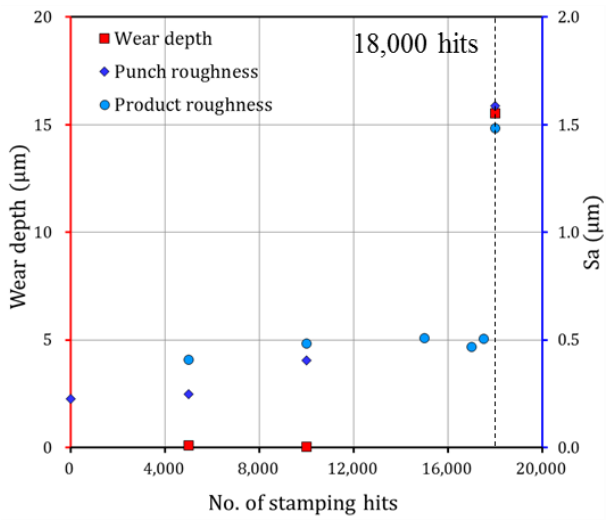
Wear depth
Punch roughness
Product roughness
18,000 hits
Wear depth (µm)
Sa (µm)
No. of stamping hits
0
4,000
8,000
12,000
16,000
20,000
0
5
10
15
20
0.0
0.5
1.0
1.5
2.0

(b)

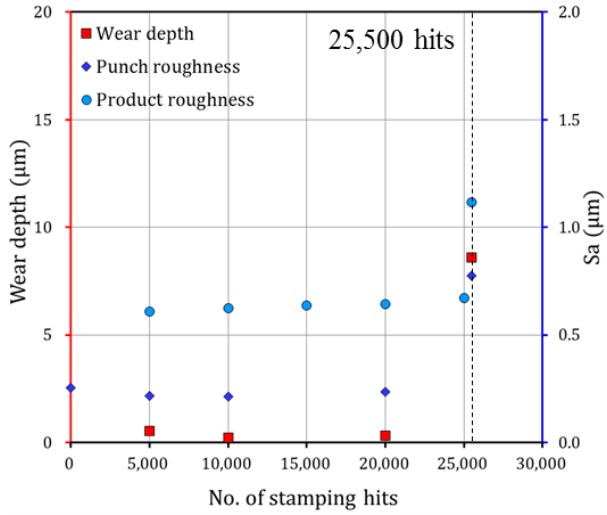

(c)

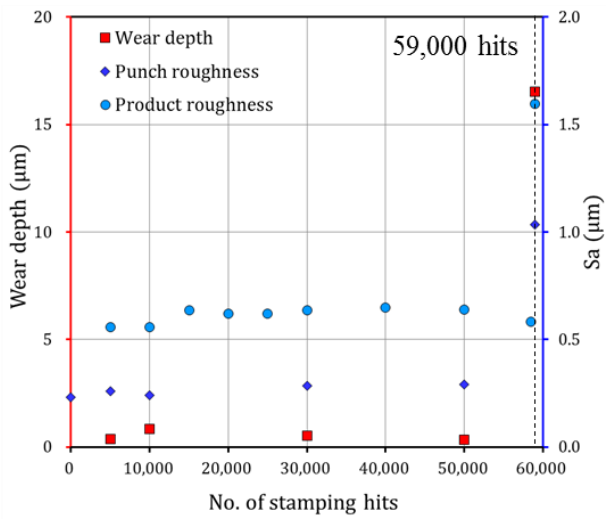

(d)

Fig. 3-14. Evolutionary wear behavior for all punches with respect to stamping hits. (a) Punch 1 (R3.0, STD-11, CrN coating), (b) Punch 2 (R5.5, STD-11, CrN coating), (c) Punch 3 (R3.0, K340, CrN coating), (d) Punch 4 (R3.0, STD-11, AlTiCrN coating)

The results of the wear tests verified that selection of the tool materials and coatings during the tool design is critical to improve the tool wear lifetime. To quantify the effect of various combinations of tool materials (STD-11 and K340) and coatings (CrN and AlTiCrN) on wear resistance, the correlation between Vickers hardness and wear resistance for Punch 1, 3, and 4 were analyzed, as illustrated in Fig. 3-15. The normal load for indentation is 0.2 kgf, which is sufficient to confirm the influence of the tool material. Punches 1, 3, and 4 have a Vickers hardness of 1,545.3, 1,609.2, and 2,647.4 $HV_{0.2}$, respectively, when loaded normally with 0.2 kgf. Because the Vickers hardness of K340 is greater than that of STD-11, the Vickers hardness of Punch 3 (1,609.2 $HV_{0.2}$) is greater than that of Punch 1 (1,545.3 $HV_{0.2}$). Because AlTiCrN coating has a higher Vickers hardness than CrN coating, Punch 4 has a higher Vickers hardness (2,647.4 $HV_{0.2}$) than Punch 1. (1,545.3 $HV_{0.2}$). The higher the Vickers hardness of the punch, the more the materials' wearing resistance. At 16,500 hits, Punch 1 (STD-11, CrN) failed. By switching from STD-11 to K340 tool material, the number of failed stamping hits increased by 54.5% (Punch 3). Additionally, by switching from CrN to AlTiCrN coatings, the number of failed stamping hits increased by 257.6% (Punch 4). The coating has a greater effect on improving the Vickers hardness of the punch than the tool material. Thus, hard coatings are more effective at

increasing wear resistance than hard tool material. Additionally, it is highly effective in establishing a design guideline for the tool wear lifetime by examining the tool's hardness characteristics for various tool materials and coatings.

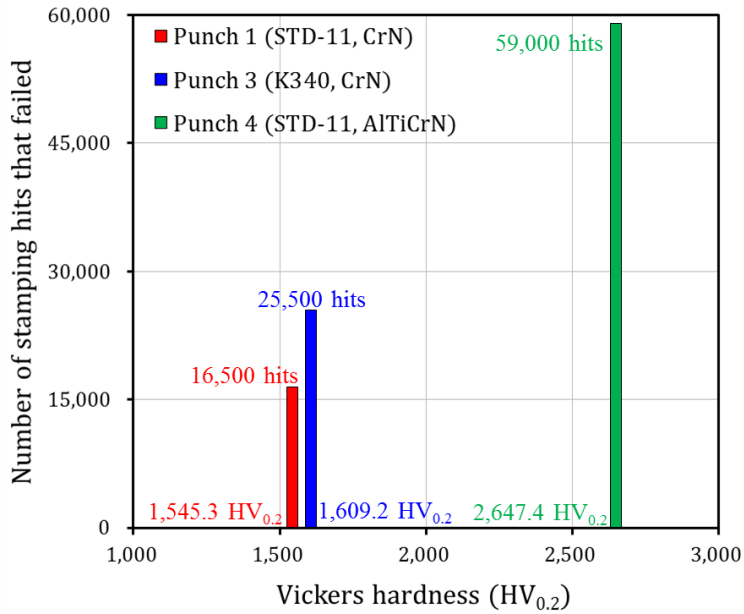

Fig. 3-15. Correlation between Vickers hardness at a normal load of 0.2 kgf and wear resistances.

4. Application to stamping analysis considering tool wear

4.1. Forming simulation

An FE simulation was conducted to predict the contact conditions on the punch surface during the stamping process, which was performed using LS-Dyna R11.0 explicit code. To reduce the computational time, the simulation was simplified to a half model using symmetric boundary conditions. Ersoy-Nürnberg et al. [42] reported that the elastic deformation of a tool is not significantly correlated to the contact pressure distribution on the tool surface. On the other hand, Pereira et al. [36] confirmed that the analytical rigid tool model ($E=\infty$) and the elastic tool model (E=205 GPa) were compared to confirm the effect of the elasticity of the tool material on the contact pressure. The maximum contact pressure of the analytical rigid tool solution was predicted to be 30% higher than that of the elastic tool solution. According to the literature [50–51], the elastic modulus of the CrN and AlTiCrN coatings are 400.0 and 469.5 GPa, respectively, so the difference in maximum contact pressure between the tool model to which the elastic modulus of the coating is applied and the analytical rigid tool model is expected to be less than 30%. Moreover, For wear simulation of complex and large parts such as automobile

components, the tools modelled with deformable solid elements require significant computational time, so rigid-body modelling of the tools is usually assumed in order to simplify the simulation model. In this sense, the tools (punch, pad, and die) were modelled with rigid bodies. They also demonstrated that when a blank was modelled with shell and solid elements, the wear simulation results for both element types were in excellent agreement with the experimental results. Thus, the blank was discretized by deformable shell elements, which also helps to reduce the computational time.

The contact characteristics on the tool surface are sensitive to the mesh quality. Thus, sensitivity of the contact interface mesh size to the contact pressure was confirmed for the punch geometry with a radius of 3.0 mm. The mesh size at the punch contact interface was evaluated for 0.2, 0.4, and 0.8 mm. To reduce computational time, the mesh refinement method was applied to the simulation model. The initial blank mesh size was 5.0 mm. By setting the mesh refinement method to 6, 5, and 4 levels, the final blank mesh size was 0.156, 0.313, and 0.625 mm for each punch mesh size case, respectively. Pad and die contact pressure prediction does not require accuracy, thus it was modelled with a relatively coarse size of 0.5 mm. FE modeling for the simulation is shown in Fig. 4-1 with the FE model details summarized in Table 4-1.

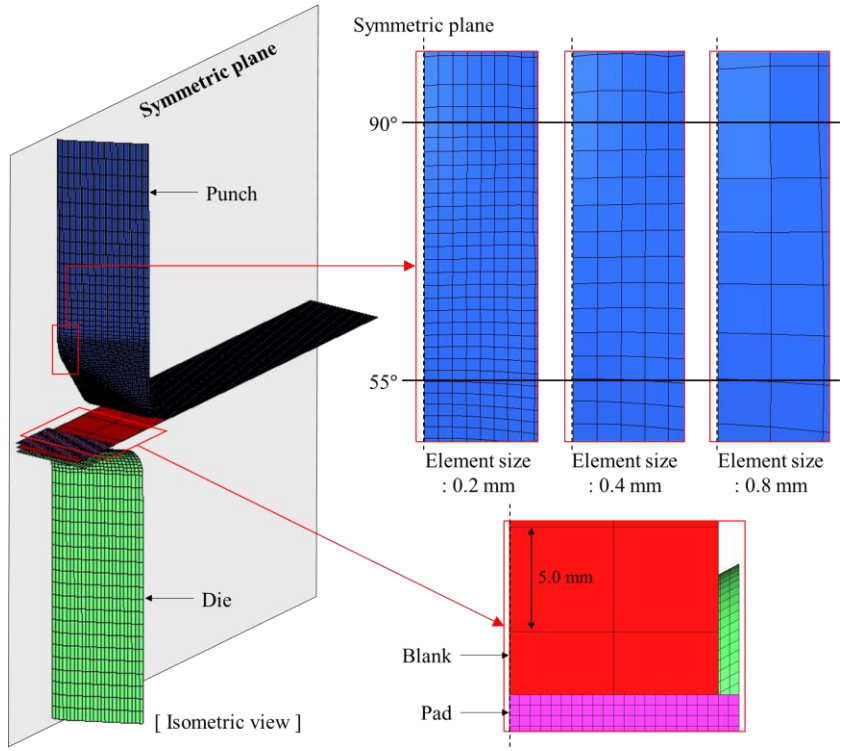

Fig. 4-1. FE modeling to evaluate mesh size sensitivity at the stamping process contact interface.

Table 4-1. FE modeling details and computational time for each element size case.

	Element size (mm)			Element type
Punch	0.2	0.4	0.8	Rigid body
Blank	0.156 (lv. 6)	0.313 (lv. 5)	0.625 (lv. 4)	Deformable shell
Pad		0.5		Rigid body
Die				
Computational time	8 h	2 h	20 min	

The number of integration points in the thickness direction of the blank was set to 5. Pereira et al. [36] confirmed that a Coulomb friction coefficient of 0.15 was appropriate to predict an accurate contact pressure distribution by comparing the experiments and numerical simulations of the channel forming process. In this study, a Coulomb friction coefficient of 0.15 was applied at the contact interface between the punch and blank because it is difficult to calculate appropriate friction coefficient by measuring the punch reaction force of the stamping process among the various metalworking operations of the employed progressive die tool. Amounts of the contact pressure generated on the contact interface are affected by the strength of the steel sheet. TRIP1180 with a thickness of 1.2 mm was used as the blank material. As

shown in Table 2-1, the 1.2-mm-thick TRIP1180 steel sheet shows the anisotropic characteristics. Therefore, Hill's 1948 yield criteria [52] were employed to consider the anisotropic plastic deformation behavior and to predict the accurate contact pressure. The anisotropic parameters of the Hill's 1948 yield criteria used in the simulation are summarized in Table 4-2. The padding force was 12.0 kN, which is sufficient to hold the sheet metal during the stamping process. The punch stroke was 35.0 mm.

Table 4-2. The anisotropic parameters of the Hill's 1948 yield criteria used in the simulation

Anisotropic parameters			
F	G	H	N
5.629×10^{-7}	6.612×10^{-7}	4.881×10^{-7}	1.810×10^{-6}

Fig. 4-2 compares the contact pressure history at a node on the punch radius where the highest contact pressure occurs to evaluate contact characteristics according to mesh sizes and predicted contact pressures for all mesh size cases are of similar magnitude. The simulation was performed on a computer with an Intel Core i7-6700 CPU and 8 GB RAM. Computational time was approximately 8 h, 2 h, and 20 min, respectively, as summarized in Table 4-1. Thus, the mesh size of 0.8 mm at the punch contact interface can effectively

reduce computational time. However, as shown in Fig. 4-1, if the mesh size at the contact interface is coarse, the number of elements between 55 and 90° on the punch radius is insufficient such that it is difficult to accurately analyze contact characteristics over the punch radius. Therefore, in the simulation cases for this study, a 0.2 mm mesh size was applied at the punch contact interface, and 0.156 mm was used for the final blank mesh size by applying six levels of the mesh refinement method, which is sufficiently refined for accurate prediction of the contact conditions on the punch surface.

Fig. 4-2. Contact pressure history comparison at a node on the punch radius where the highest contact pressure occurs to evaluate contact characteristics according to element sizes.

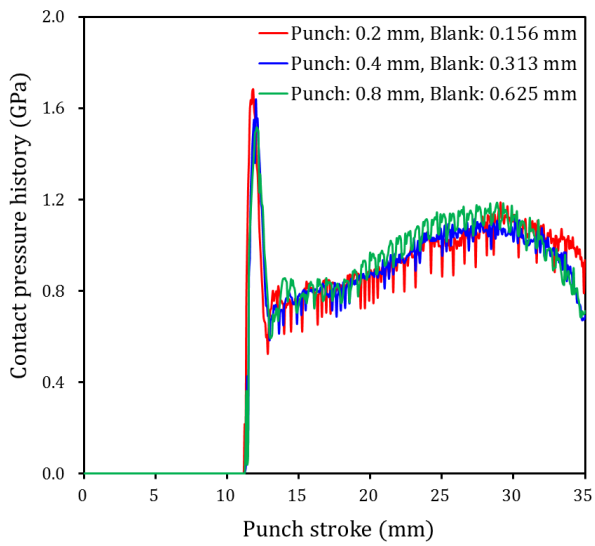

In sheet metal forming, the contact pressure and sliding distance are the most significant factors influencing tool wear [36, 43, 53–55]. Thus, these two

factors on the punch radius were investigated. To understand the time-dependent evolution of contact pressure along the punch radius during the stamping process, Fig. 4-3 shows contour plots of the contact pressure over the punch radius during stamping. The ordinate represents the punch stroke level during stamping, while the abscissa represents the angle on the punch radius. As shown in Fig. 4-3, the contact pressure levels over the radius of the R3.0 punch are higher than that over the radius of the R5.5 punch. Fig. 4-4(a) plots the maximum contact pressure with respect to the punch stroke level for each punch shape. A highly localized contact pressure was distributed on both punch shapes between approximately 10.0 mm and 13.0 mm of the punch stroke. In this punch stroke range, the maximum contact pressures acting on the R3.0 and R5.5 punches are 1.707 GPa and 1.372 GPa, respectively. These maximum contact pressures move along the punch radius transiently from 55.0° to approximately 83.0° for both the R3.0 and R5.5 punches, as shown in Fig. 4-4(b), which plots the angular location of the maximum contact pressure as the punch stroke progresses. A relatively high contact pressure is experienced over most of the angular range of the punch radius during the short punch strokes. Pereira [36] defined the initial region of the stamping process as a transient region where the angular location and magnitude of the contact pressure on the punch radius change significantly; this region is

between approximately 10.0 and 13.0 mm of the punch stroke in the present study. In this transient region, a blank is formed and wrapped over the punch radius such that a transient change in the contact pressure response occurs with the changes in the contact conditions of the punch radius. As shown in Fig. 4-3, a steady and relatively lower contact pressure than that of the transient region is distributed over the punch radius for both the R3.0 and R5.5 punches between approximately 13.0 mm and 35.0 mm of the punch stroke. Pereira [36] referred to the region with such a steady contact pressure response as the steady-state region. Fig. 4-4(a) illustrates the magnitude of the maximum contact pressure in this punch stroke range in more detail. A relatively steady contact pressure was observed for both punches. In addition, the contact pressure of the R3.0 punch was approximately 0.15 GPa higher than that of the R5.5 punch. In the steady-state region, the relatively high contact pressure for each punch stroke is concentrated on approximately 67.3° and 72.9° on the punch radius for the R3.0 and R5.5 punches, respectively, as shown in Fig. 4-4(b). Although the geometrical wrapping angle of the blank is 90° for both punches, the contact angle on the punch radius of the R5.5 punch is larger. The difference in contact angle on the punch radius can be inferred from the geometrical difference between the R3.0 and R5.5 punches. Bang et al. [24] revealed that the wear of a coated tool is caused by the

interaction between the contact pressure and the sliding distance in the stamping process. Therefore, the transient region, where the highly localized contact pressure and short sliding distance occur, is not considered to have a critical effect on the wear response. Therefore, tool wear is expected to occur in the steady-state region. Fig. 4-4(c) shows the contact conditions at approximately 67.3° and 72.9° on the punch radius for the R3.0 and R5.5 punches, respectively, where the highest contact pressure and longest sliding distance in the steady-state region occur. Because the curvature of the R3.0 punch is sharper than that of R5.5 punch, the R3.0 punch has a higher contact pressure.

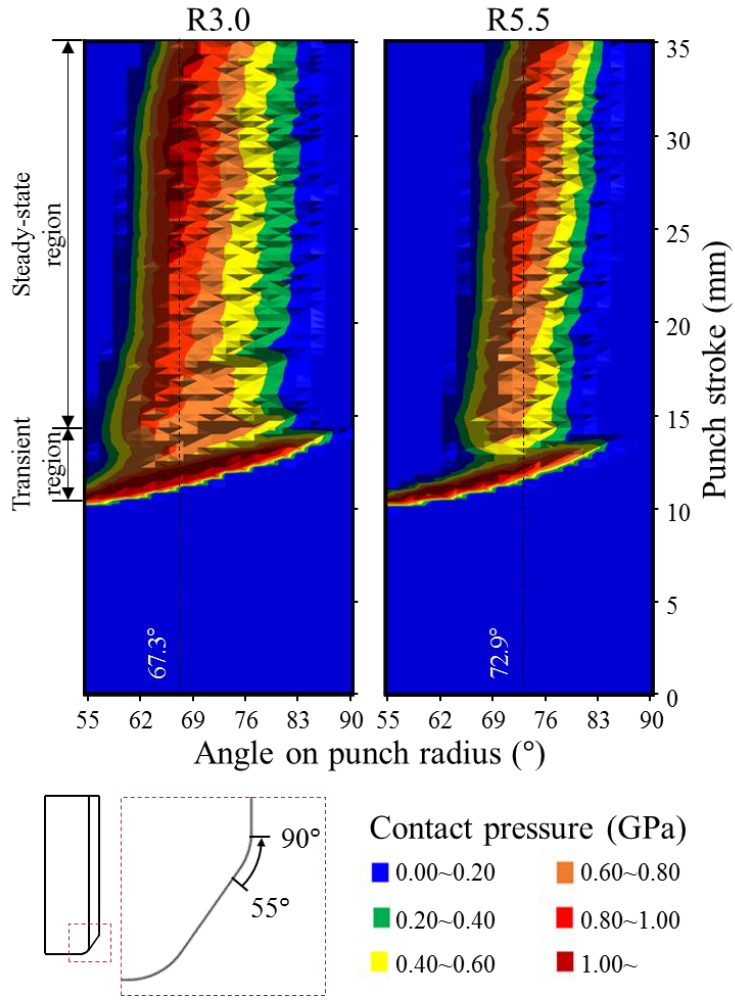

Fig. 4-3. Time-dependent evolution of contact pressure on the punch radius during the stamping process.

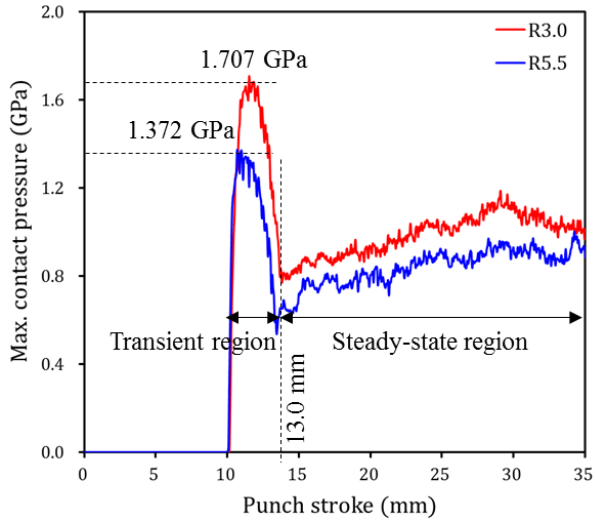
R3.0
R5.5
1.707 GPa
1.372 GPa
Transient region
Steady-state region
13.0 mm
Max. contact pressure (GPa)
Punch stroke (mm)

(a)

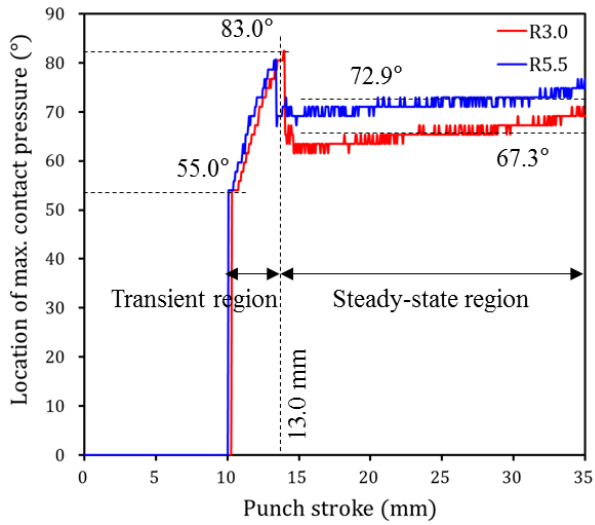
R3.0
R5.5
83.0°
72.9°
67.3°
55.0°
Transient region
Steady-state region
13.0 mm
Location of max. contact pressure (°)
Punch stroke (mm)

(b)

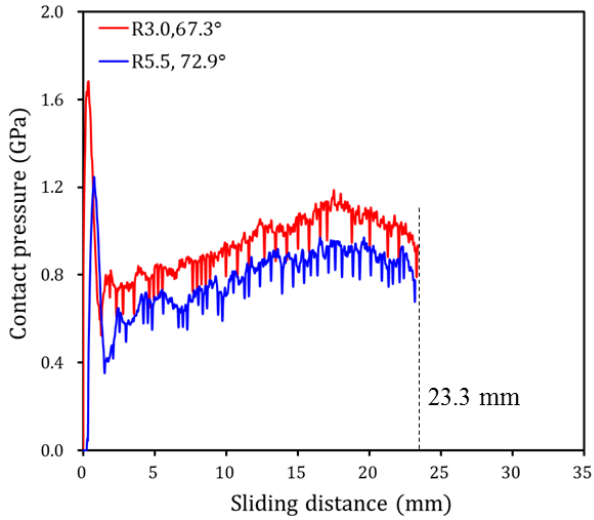

(c)

Fig. 4-4. Contact conditions on the punch radius for the R3.0 and R5.5 punches. (a) maximum contact pressure with respect to the progression of the punch stroke, (b) location of the maximum contact pressure with respect to the progression of the punch stroke, (c) contact conditions at approximately 67.3° and 72.9° on the punch radius for the R3.0 and R5.5 punches, respectively

4.2. Tool wear prediction model

Archard's wear model [48] is the most widely used model to predict the tool wear in sheet metal forming, and it is also built into LS-Dyna, as expressed in Eq. (4.1):

$$w = k\frac{pl}{H} \tag{4.1}$$

In Eq. (4.1), the wear depth w is directly proportional to the contact interface pressure p and the relative sliding distance l on the contact interface, and it is inversely proportional to the hardness of the wearing material H. k is a dimensionless wear coefficient. Eq. (4.1) needs to be discretized in the elemental form to be implemented to FE simulations. The wear depth change $\dot{w}$ at a certain time t can be calculated as follows:

$$\dot{w} = k\frac{p_t v_t}{H} \tag{4.2}$$

where p_t is the contact interface pressure at a certain time t and v_t is the sliding velocity at a certain time t. By integrating Eq. (4.2) over time duration of the stamping process, the wear depth w on the contact interface can be calculated as follows:

$$w = \frac{k}{H}\int (p_t v_t)dt \tag{4.3}$$

Because the wear depth was close to 0 before failure initiation, the contact pressure and the sliding distance on the contact interface were considered to be constant. Therefore, the wear depth predicted by Eq. (4.3) is linear. As

shown in the wear test results in Fig. 3-2, the evolutionary wear behavior with respect to the strokes is not linear. Therefore, a nonlinear equation from a modified form of Archard's wear model is proposed as follows:

$$w = \frac{k(n)}{H} \int (p_t v_t) dt \tag{4.4}$$

where $k(n)$ is the dimensionless wear coefficient as a function of the number of strokes n. Here, $k(n)$ is a variable that can express the wear behavior with respect to the number of strokes. The wear test results in Fig. 3-2 show that wear depth is close to 0 before failure. When failure occurs, the wear depth increases rapidly. In order for the analytical solution (Eq. 4.4) to express the evolutionary wear behavior before and after failure and accurately simulate the experimental results (Fig. 3-2), it is necessary to define $k(n)$ for each punch. An exponential function was used for $k(n)$ to approximate the rapidly increasing wear behavior with respect to strokes after failure initiation. If $k(n)$ of Eq. 4.4 is not defined, the wear behavior with respect to strokes is predicted linearly. As shown in Fig. 4-5, it can be confirmed that the analytical solution (Eq. 4.4) accurately predicts the experimental wear data due to the definition of $k(n)$. The fitted dimensionless wear coefficient $k(n)$ for CrN- and AlTiCrN-coated punches are as follows:

$$k(n)_{CrN} = Aexp(Bn) = 5.20 \times 10^{-5} exp(5.855 \times 10^{-4} n) \quad (4.5)$$

$$k(n)_{AlTiCrN} = Aexp(Bn) = 3.05 \times 10^{-15} exp(5.855 \times 10^{-4} n) \quad (4.6)$$

The R squared (R^2) is equal to 0.9999 for both exponential regressions. The Root Mean Square Deviation (RMSD) is 3.214×10^{-5} and 5.855×10^{-4} for each exponential regression, respectively. A of $k(n)$ is related to the delay of the failure initiation, and B of $k(n)$ means the rapidly increasing wear behavior after failure. In this study, the same value of 5.855×10^{-4} was used for B of $k(n)$ due to the insufficient wear depth results to describe the wear behavior after failure initiation. The $k(n)$ of the AlTiCrN-coated punch is smaller than that of the CrN-coated punch, which means that as the wear test progressed, the wear rate of the AlTiCrN-coated punch was slower. Thus, it is possible to simulate a failure initiation behavior occurring later in the AlTiCrN-coated punch.

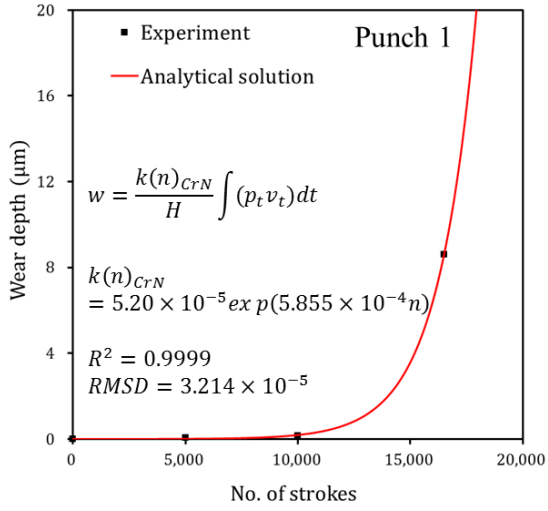
Experiment
Punch 1
Analytical solution
$w = \frac{k(n)_{CrN}}{H}\int (p_t v_t)dt$
$k(n)_{CrN} = 5.20 \times 10^{-5} exp(5.855 \times 10^{-4} n)$
$R^2 = 0.9999$
$RMSD = 3.214 \times 10^{-5}$
Wear depth (μm)
No. of strokes
0
4
8
12
16
20
0
5,000
10,000
15,000
20,000

(a)

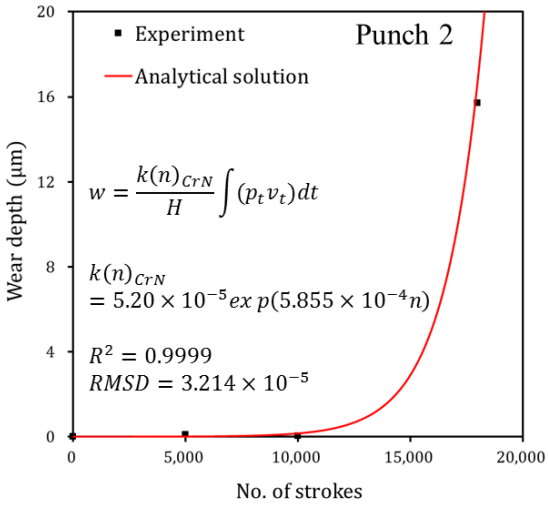
Experiment
Punch 2
Analytical solution
$w = \frac{k(n)_{CrN}}{H}\int (p_t v_t)dt$
$k(n)_{CrN} = 5.20 \times 10^{-5} exp(5.855 \times 10^{-4} n)$
$R^2 = 0.9999$
$RMSD = 3.214 \times 10^{-5}$
Wear depth (μm)
No. of strokes
0
4
8
12
16
20
0
5,000
10,000
15,000
20,000

(b)

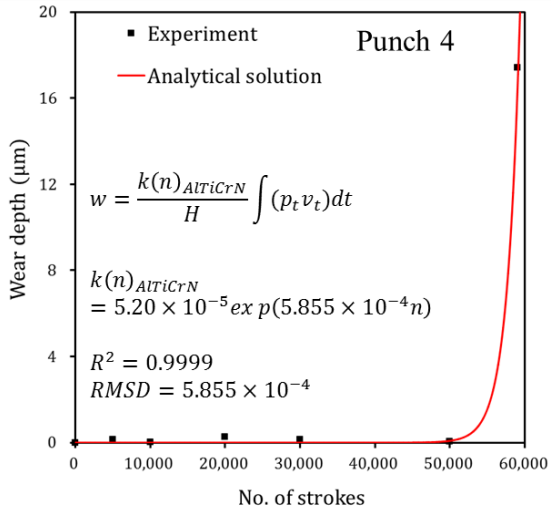

(c)

Fig. 4-5. Definition of dimensionless wear coefficient $k(n)$ of the analytical solution (Equation 4) to accurately predict the evolutionary wear behavior of experimental wear data: (a) Punch 1 with a radius of 3.0 mm coated with PVD CrN, (b) Punch 2 with a radius of 5.5 mm coated with PVD CrN, and (c) Punch 3 with a radius of 3.0 mm coated with PVD AlTiCrN.

4.3. Wear simulation

Based on the constructed wear equation, a wear simulation was performed by following the process shown in Fig. 4-6. First, the wear-related variables, hardness H, and dimensionless wear coefficient k, are entered in the "CONTACT_ADD_WEAR" card of the simulation keyword file. The hardness H is a value corresponding to each coating hardness. Although the dimensionless wear coefficient k is a function of the number of strokes n,

as expressed in Eq. (4.5)−(4.6), a value of 1 is set, as described in detail later. By performing numerical analysis with the constructed input file, the wear depth w_0 from Eq. (4.4) is computed. Because $k(n)$ is set to 1, the evolutionary wear behavior with respect to the number of strokes is not taken into account in the wear depth information. The computed wear depth information is contained in the dynain file. To perform the wear simulation and initialize the wear depth for the wear simulation process, the dynain file with wear depth information is included in the original input file. To predict the tool wear behavior, continuously track the wear status, and visualize the worn tool geometry with respect to the number of strokes, the "Wear analysis" application of LS-PrePost was used by reading in the input file including the dynain file. The scale factor F in the "Wear analysis" application was used to define the rapid increase in wear depth after failure initiation, and predict the evolutionary wear behavior with respect to the strokes. The scale factor F is defined as a change in wear properties and characteristics with respect to the wear depth as wear progresses, and can be explained by the difference in wear depth between $n + 1$ and n strokes, as expressed as follows:

$$Scale\ factor\ (F) = k(n+1) - k(n) \tag{4.7}$$

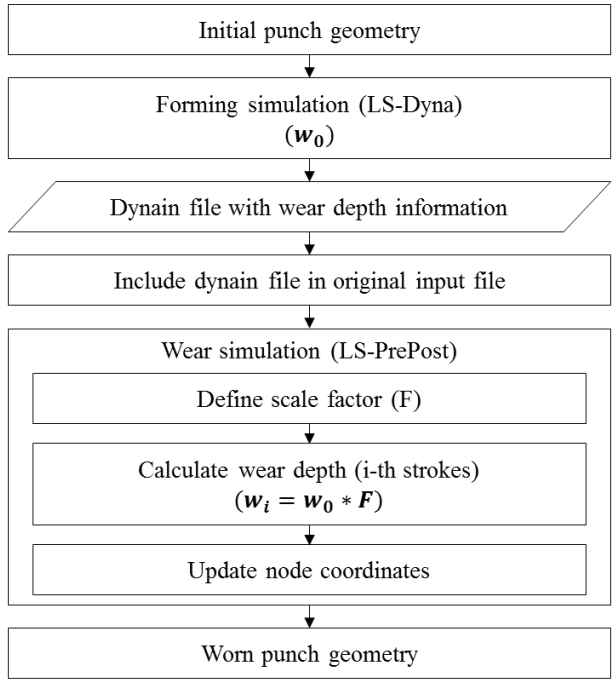

Fig. 4-6. Process of wear simulation based on the modified Archard's wear model.

Fig. 4-7 plots the scale factors F for each stamping punch condition. The abscissa is the analytical solution for the wear depth calculated from Eq. (4.4) for each stamping punch condition. The ordinate is the change in the dimensionless wear coefficient $k(n)$ with respect to the change in the number of strokes n. In the case of the CrN-coated punches, the $k(n)_{CrN}$ (red line) of the R3.0 punch is smaller than that (blue line) of the R5.5 punch at the same wear depth value. That is, for the punches with the same surface hardness, to calculate the same wear depth, $k(n)$ is inversely proportional to the contact pressure and sliding distance, which can be calculated from Eq.

(4.4). Therefore, the scale factor of the R5.5 punch, which has a smaller contact pressure, is larger than that of the R3.0 punch. In the case of punches with the R3.0 punch shape, the $k(n)_{AlTiCrN}$ (green line) of the AlTiCrN-coated punch is larger than the $k(n)_{CrN}$ (red line) of the CrN-coated punch. For punches subjected to the same contact conditions, it can be confirmed from Eq. (4.4) that $k(n)$ is proportional to the surface hardness to calculate the same wear depth. This phenomenon is reflected in the simulation by inputting the wear depth versus scale factor F into the "Wear analysis" application in the piecewise linear format. The wear depth w_i from i-th strokes can be calculated by multiplying the scale factor F by the wear depth w_0 from the forming simulation, and the amount and location of the punch wear can be visually confirmed in LS-PrePost. Therefore, this wear simulation method using the scale factor F does not need to update the geometry and calculate the accumulated wear from the previous iteration of the wear simulation.

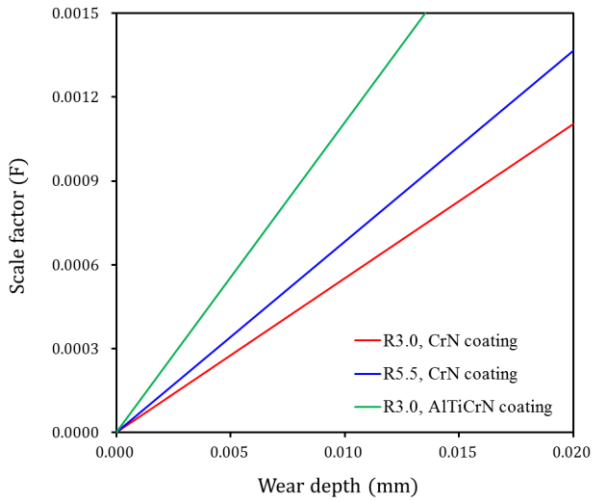

Fig. 4-7. Scale factors for each punch condition.

As shown in Fig. 4-8, in the general wear simulation, the modified geometry should be updated from the geometry predicted in the previous iteration of the wear simulation to predict the accumulated wear amount up to the desired number of strokes. This process takes a large amount of time to repeat up to the desired iteration. In contrast, the proposed wear simulation procedure using a scale factor F representing the change in wear properties with respect to the wear depth eliminates the need for repeating geometry updates from previous iterations of the wear simulation.

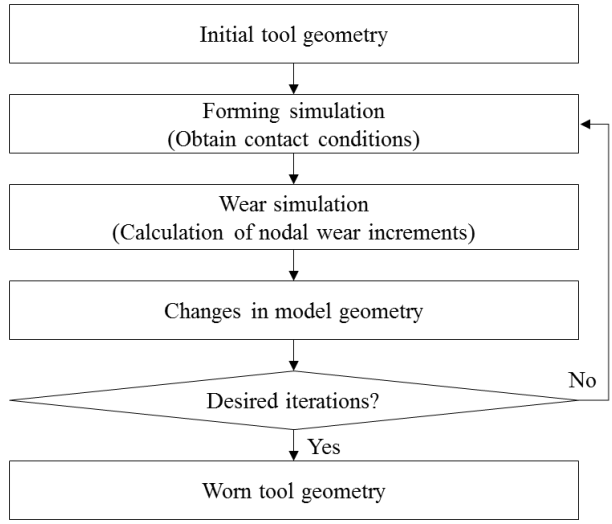

Fig. 4-8. General wear simulation method [22, 42, 56].

It was assumed that the contact pressure, sliding distance, and hardness on the contact interface of the punch were constant, because the wear depth was close to 0 before failure initiation. This assumption was considered to be appropriate from the experimental results as shown in Fig. 3-2. However, the wear depth just before failure initiation was not measured for all punches, so the constructed wear equation may not be accurate in predicting the wear depth just before failure initiation and it is necessary to verify the wear behavior just prior to failure for more accurate wear prediction.

4.4. Verification of wear simulation

Fig. 4-9 confirmed that the constructed wear simulation method can reliably predict the evolutionary wear behavior of sheet metal forming. The

analytical solution and simulation results based on the revised Archard's wear model were compared with the experimental results. It can be confirmed that the analytical solution and simulation results based on the revised Archard's wear model accurately simulate the evolutionary wear behaviors of experimental results for each punch. The results obtained using the proposed wear simulation process are quantitatively reliable in predicting the rapidly increasing wear depth behavior after failure and in determining the number of strokes at which failure occurs. Fig. 4-10 illustrates the predicted wear distributions and worn surface conditions on the punch radius for each punch condition after the failure; the predicted wear distribution confirms the amount and location of the computed wear depth. For all punches, predicted wear is concentrated on the punch radius. The wear of Punch 2 (see Fig. 4-10(b)) is more widely distributed than Punch 1 and Punch 3 (see Fig. 4-10(a) and Fig. 4-10(c)) because the shape of Punch 2 has a larger radius of 5.5 mm. The predicted wear is localized on the specific angular location, but punch surface conditions after wear test show long wear track in the sliding contact direction. The reason for this is that the wear is continuously propagated in the sliding contact direction, after wear is initiated at the specific angular location. To check the accuracy of the amount and angular location of the predicted wear distribution, Fig. 4-11 compares the wear depth for

experimental and simulation results after the failure occurred. The wear location confirmed in the experiments is approximately 88° on the punch radius for all three punch conditions. However, the angular location of the maximum wear depth predicted from the simulation was approximately 15°–20° ahead of that of the experiments. As the punch stroke progresses, the steel sheet comes into contact with the punch at 55° first and then in the 90° direction. Therefore, it is inferred that during the stamping process, wear debris generated by the high contact pressure at about 70° of the punch radius moves in the 90° direction, and severe wear occurred at approximately 88° on the punch radius due to the wear debris. To verify the simulation accuracy, Fig. 4-12 compare the difference in maximum wear depths between experiments and simulations. For each punch, the predicted maximum wear depth after the failure showed differences of 6.2, 7.1, and 5.8%, respectively, from the experiments. Therefore, it was confirmed that the proposed wear simulation method is reliable in evaluating the wear depth and lifetime of stamping tools.

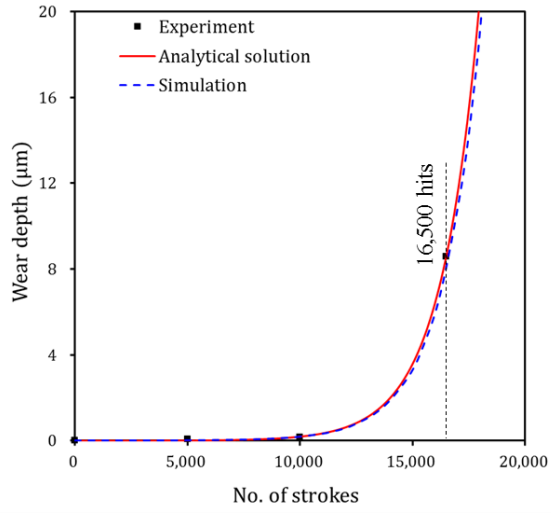
Experiment
Analytical solution
Simulation
16,500 hits
Wear depth (μm)
No. of strokes
0
4
8
12
16
20
0
5,000
10,000
15,000
20,000

(a)

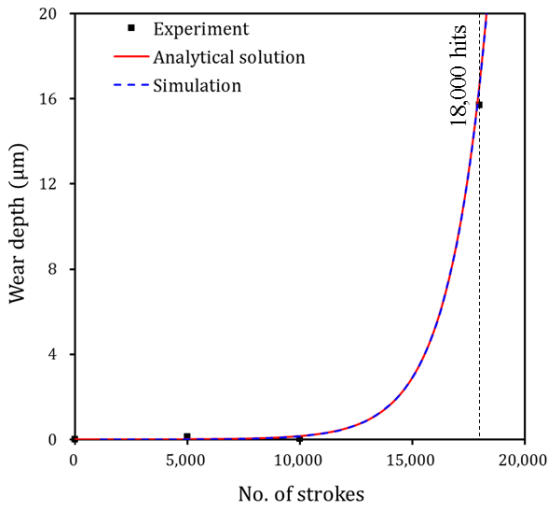
Experiment
Analytical solution
Simulation
18,000 hits
Wear depth (μm)
No. of strokes
0
4
8
12
16
20
0
5,000
10,000
15,000
20,000

(b)

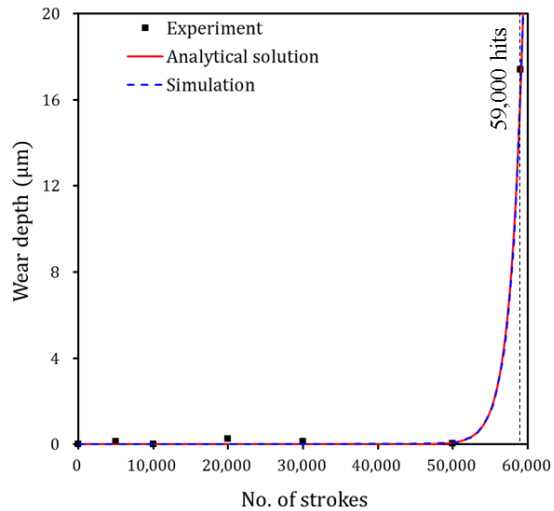

(c)

Fig. 4-9. Comparison of the experimental results, analytical solution, and simulation results based on the modified Archard's wear model with respect to the number of strokes. (a) Punch 1 (R3.0, STD-11, CrN coating), (b) Punch 2 (R5.5, STD-11, CrN coating), (c) Punch 4 (R3.0, STD-11, AlTiCrN coating)

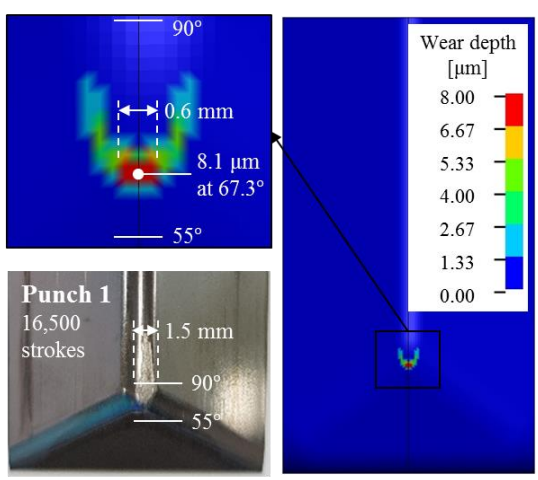

(a)

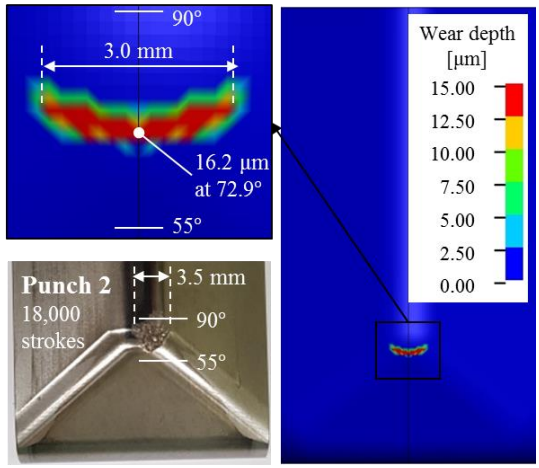

(b)

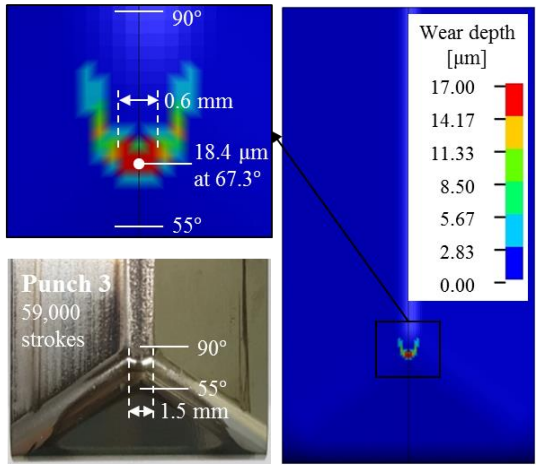

(c)

Fig. 4-10. Predicted wear distributions and worn surface conditions on the punch surface after the failure. (a) Punch 1 (R3.0, STD-11, CrN coating), (b) Punch 2 (R5.5, STD-11, CrN coating), (c) Punch 4 (R3.0, STD-11, AlTiCrN coating)

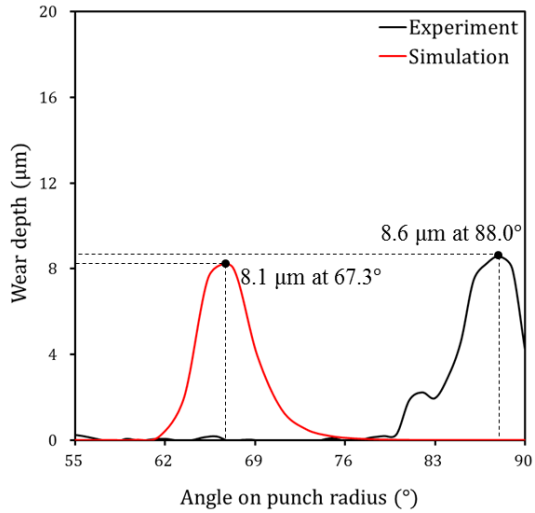
Experiment
Simulation
8.6 µm at 88.0°
8.1 µm at 67.3°
Wear depth (µm)
Angle on punch radius (°)
0
4
8
12
16
20
55
62
69
76
83
90

(a)

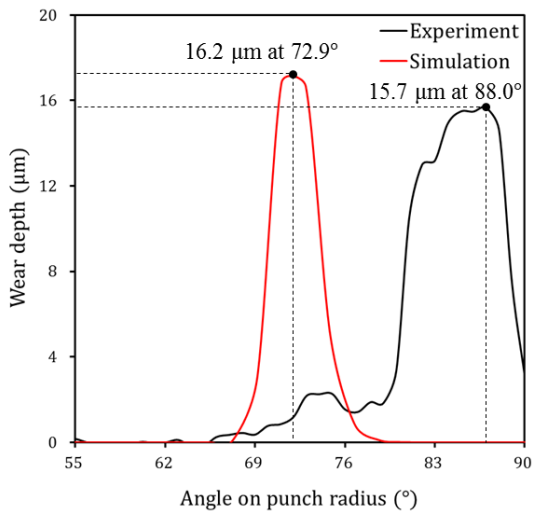
Experiment
Simulation
16.2 µm at 72.9°
15.7 µm at 88.0°
Wear depth (µm)
Angle on punch radius (°)
0
4
8
12
16
20
55
62
69
76
83
90

(b)

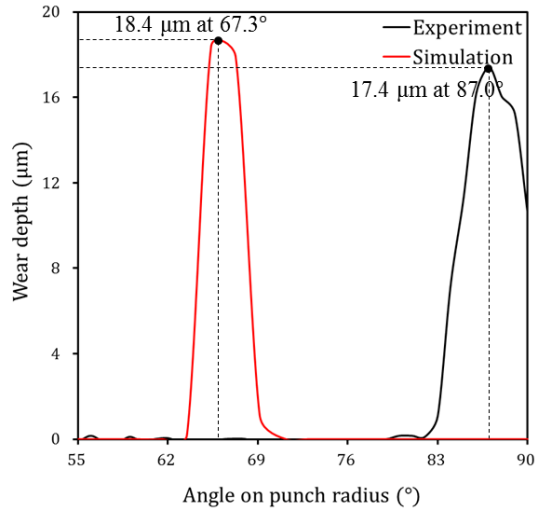

(c)

Fig. 4-11. Wear depth on the punch radius obtained from experiments and simulations after the failure. (a) Punch 1 (R3.0, STD-11, CrN coating), (b) Punch 2 (R5.5, STD-11, CrN coating), (c) Punch 4 (R3.0, STD-11, AlTiCrN coating)

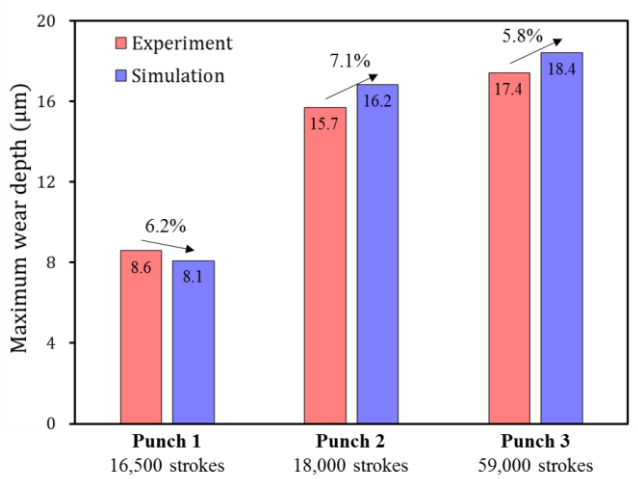

Fig. 4-12. Difference in maximum wear depths between experiments and simulations.

4.5. Discussion

The Archard's wear model was compared with experimental results of CrN-coated punches to confirm the limitations of predicting evolutionary wear behavior in sheet metal forming. The elemental form of the Archard's wear model for CrN-coated punches was fitted using experimental wear data, subsequently; the dimensionless wear coefficient of 0.074 was obtained, as follows:

$$w_{CrN} = \frac{0.074}{2{,}105} \int (p_t v_t) dt \tag{4.8}$$

The simulation results based on Eq. (4.8) were obtained for CrN-coated punches, and compared with experimental and simulation results based on the modified Archard's wear model, as shown in Fig. 4-13. Punch 1 (CrN-coated punch with a radius of 3.0 mm) failed after 16,500 strokes and the wear depth measured was 8.6 μm. However, the predicted wear depth based on the Archard's wear model is 12.9 μm. For Punch 2 (CrN-coated punch with a radius of 5.5 mm), failure occurred after 18,000 strokes, and the wear depth measured was 17.4 μm. The predicted wear depth at 18,000 strokes based on the Archard's wear model was 11.4 μm. It can be observed that wear depth predicted by the Archard's wear model in terms of the number of strokes at

which failure occurred, significantly differed from experimental results. In addition, the experimental and simulation results based on the modified Archard's wear model demonstrated no wear at 5,000 and 10,000 strokes (i.e. before failure). It was confirmed that the Archard's wear model has limitations in simulating non-linear wear behavior of the tool in sheet metal forming.

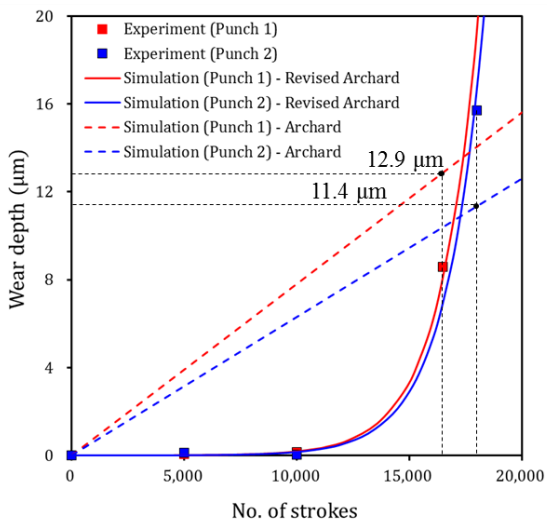

Fig. 4-13. Simulation results based on Archard's wear model for CrN-coated punches.

Tool wear during the press forming process leads to reduced product quality. From the results of the Punch 1 wear test, it was confirmed that although the wear depth was 8.6 μm, severe scratches occurred on the product surface. The contact pressures of the formed product were compared when formed with punch geometry without wear and with worn punch geometry. Fig. 4-14(a)

shows the contact pressure of the product formed with punch geometry without wear and worn punch geometry. It can be observed that the contact pressure formed with punch geometry without wear is higher than that formed with worn geometry in the middle region of the product in contact with the curvature region of the punch. Fig. 4-14(b) plots the contact pressure in the middle region of the product (dotted line), which is in contact with the punch curvature region. The contact pressure of the product formed with punch geometry without wear (red solid line) is higher than that with worn punch geometry (red dash line) in a product length of approximately 3 to 10 mm. To confirm the effect of this minor wear depth on product deformation shapes, the effective plastic strain and stress of the formed products were compared when formed with punch geometry without wear and with worn punch geometry. Fig. 4-15(a) shows the effective plastic strain of the product formed with punch geometry without wear and with worn punch geometry. It can be observed that the effective plastic strain of the product formed with punch geometry without wear is higher than that with worn punch geometry in the middle region of the product in contact with the curvature region of the punch. As shown in Fig. 4-15(b), the effective plastic stress of the product formed with punch geometry without wear is also higher in the middle region of the product. To quantitatively compare conditions of the product formed with

punch geometry without wear and with worn punch geometry, Fig. 4-15(c) plots the effective plastic strain and stress in the middle region of the product (dotted line), which is in contact with the punch curvature region. The effective plastic strain of the product formed with punch geometry without wear (red solid line) is approximately 0.4 in the range of approximately 5 to 10 mm in product length, which is twice higher than that with worn punch geometry (red dash line). The effective plastic stress of the product formed with punch geometry without wear (blue solid line) is higher than that formed with worn punch geometry (blue dash line) in a product length of approximately 3 to 14 mm. The effective plastic strain and stress of the product decreased after failure, because the radius of the curvature region of the punch increased owing to wear.

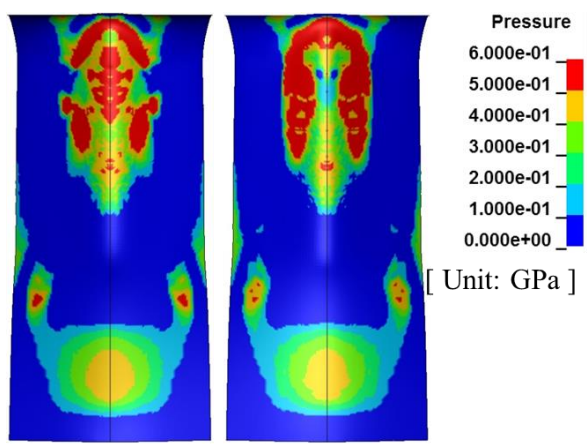

Formed with punch geometry without wear

Formed with worn punch geometry

(a)

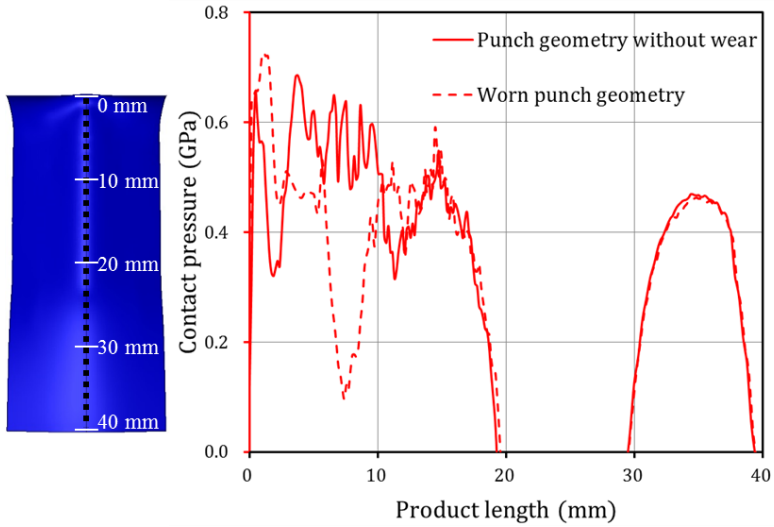

(b)

Fig. 4-14. Contact pressure of the product formed with punch geometry without wear and with worn punch geometry. (a) contour plot of contact pressure, (b) quantitative comparison of contact pressure

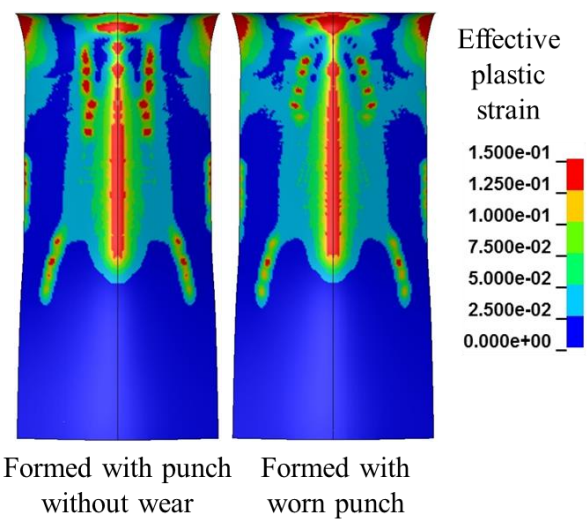

(a)

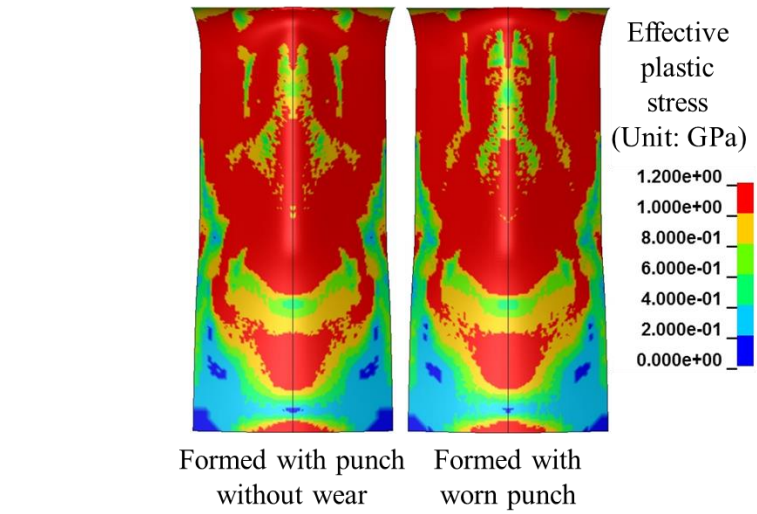

(b)

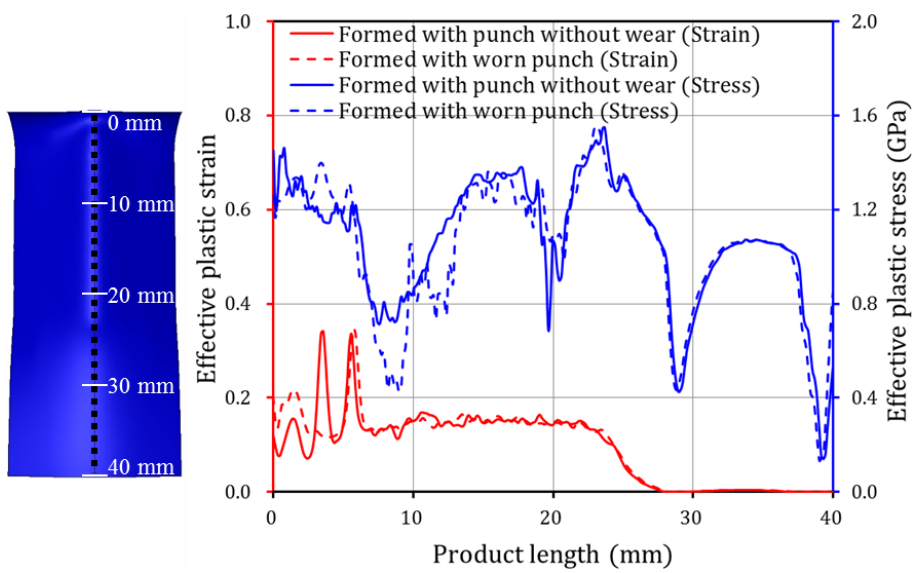

(c)

Fig. 4-15. Effective plastic strain and stress of the product formed with punch geometry without wear and with worn punch geometry. (a) contour plot of effective plastic strain, (b) contour plot of effective plastic stress, (c) quantitative comparison of effective plastic stress and strain

5. Tool wear prediction in forming an automotive part

In this chapter, the proposed tool wear prediction methodology was evaluated by applying the modified Archard's wear model to forming an automotive part to predict the tool wear behavior, and confirm the amount and location of the tool wear. In addition, the results of applying the Archard's wear model to forming the automotive part were also compared with that of the modified Archard's wear model to evaluate the accuracy of the tool wear prediction model.

5.1. Simulation setup

The automotive part used in the finite element simulation is a reinforced center floor side to which ultra-high strength steel sheets is applied to increase the crashworthiness. Forming simulation of the reinforced center floor side was conducted by using LS-Dyna R11.0 explicit code. Fig. 5-1 illustrates the geometries of tools and initial sheet blank. The sheet material used for the simulation is a 1.2 mm uncoated TRIP steel sheet with a tensile strength of 1180 MPa (TRIP1180), as summarized in Table 2-1. The anisotropic parameters of the Hill's 1948 yield criteria were applied to the simulation model to consider the anisotropic plastic deformation behavior, as summarized in Table 4-2. The wear resistance of CrN-coated tool with Vickers hardness values of 2,105.9 ± 15.5

$HV_{0.08}$. The blank holing force (BHF) of 50 ton was applied. The detailed FE simulation conditions are summarized in Table 5-1.

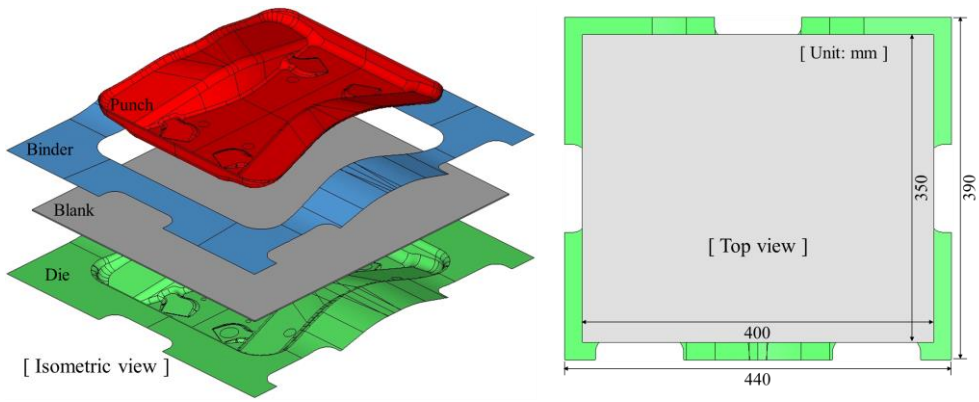

Fig. 5-1. Geometries of simulation model for forming the reinforced center floor side

Table 5-1. Detailed descriptions of forming simulation of the reinforced center floor side.

Blank material	TRIP1180 1.2t
Yield criteria	Hill's 1948
Blank holding force (BHF)	50 ton
Friction coefficient	0.15
Blank size	400 X 350 mm

As shown in Fig. 4-2, the predicted contact pressures for all mesh size cases are similar. Therefore, in order to efficiently reduce the computational time, the mesh size at the shoulder radius of the punch and die, where high contact pressure and large sliding distance are expected during forming, was applied to 0.8 mm. The final mesh size of the blank is 0.625 mm by setting the mesh refinement method to 4 levels. Binder was modelled with a relatively coarse mesh size of 5.0 mm, because its contact pressure prediction do not need to be accurate. FE modeling for the simulation is shown in Fig. 5-2 with the FE model details summarized in Table 5-2.

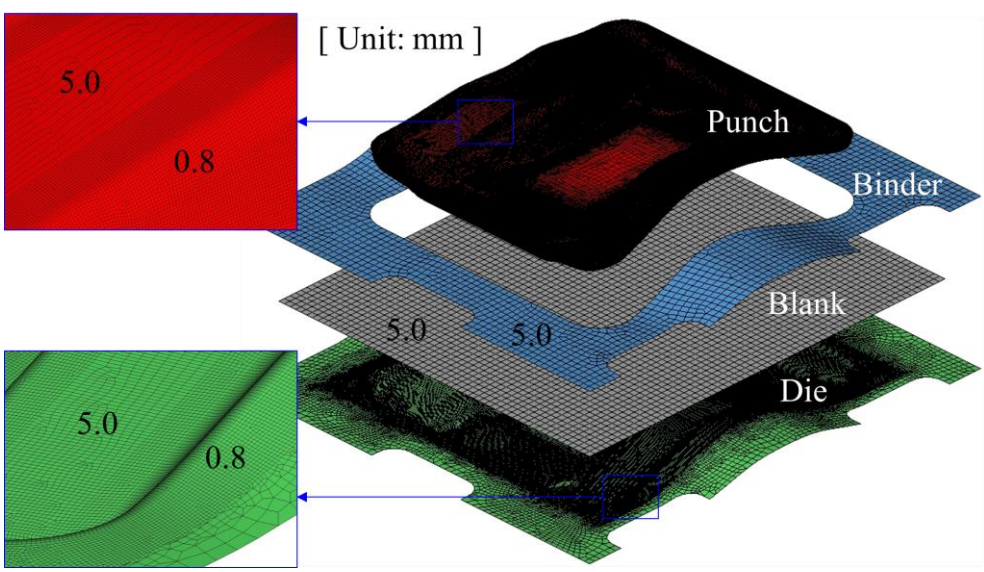

Fig. 5-2. Geometries for forming the reinforced center floor side

Table 5-2. FE modeling details for simulation model of the reinforced center floor side.

	Element size (mm)	Element type	Number of elements
Blank	0.625 (lv. 4)	Deformable shell	3,584
Binder	5.0	Rigid body	2,092
Punch	0.8	Rigid body	138,466
Die	0.8	Rigid body	116,482
Total number of elements			260,624

5.2. Tool wear prediction

The contact conditions at the die-workpiece contact interface was predicted in forming simulation of the reinforced center floor side. As shown in Fig. 5-3, the maximum contact pressure was predicted to be approximately 1.5 GPa at the sharp die corner with the smallest curvature radius of 1.6 mm. At the regions with a curvature radius of 7.2 mm, which was expected to experience large sliding, a contact pressure of approximately 0.5 GPa was predicted. As shown in Fig. 5-4, the sliding distance on the die was also evaluated. The predicted sliding distance for the sharp die corner with a curvature radius of 1.6 mm was approximately 0.5 mm. At the die corner with a curvature radius of 7.2 mm, a maximum sliding distance of approximately 14.5 mm was predicted.

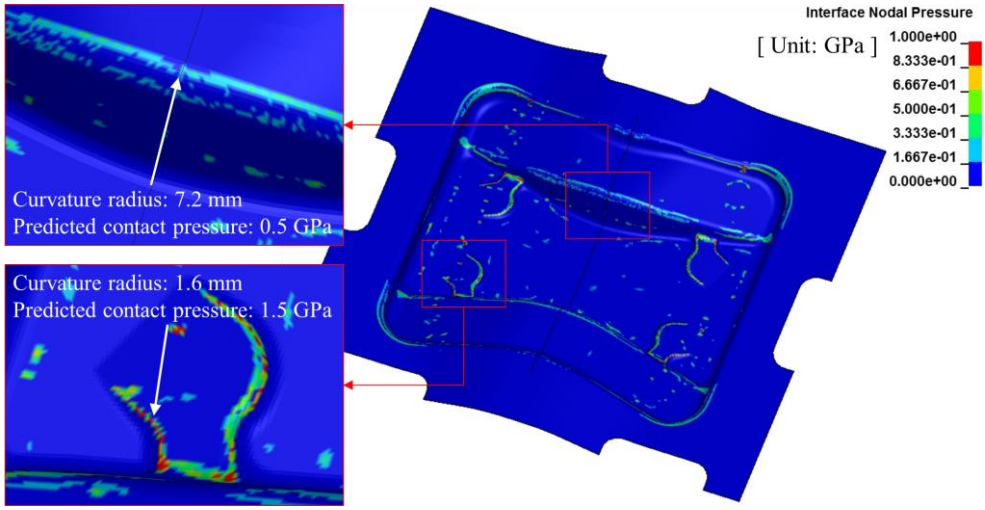

Fig. 5-3. Contact pressure distribution on the die

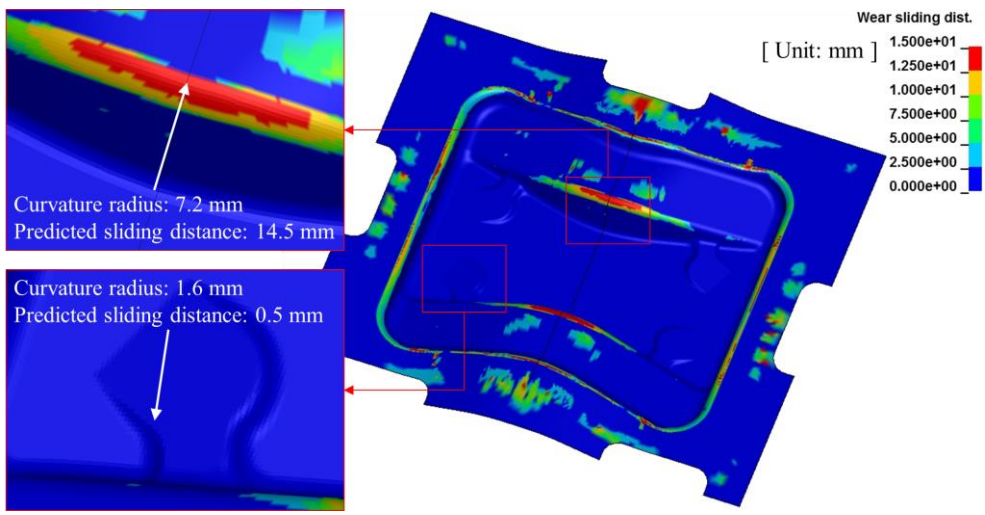

Fig. 5-4. Sliding distance distribution on the die

The modified Archard's wear model was applied to the forming simulation of the reinforced center floor side to predict the amount and location of the tool wear, and continuously track the wear status with respect to the number of strokes. Fig. 5-5 illustrates the amount and location of the wear on the die

surface after 20,000 strokes. The maximum wear depth was predicted to be 20.49 μm at the die corner with a curvature radius of 7.2 mm. Fig. 5-6 shows the contact conditions at the die corner where the maximum wear depth is predicted. Although the contact pressure is relatively low at approximately 0.5 GPa, a lot of wear occurs because of the large sliding distance of 14.5 mm.

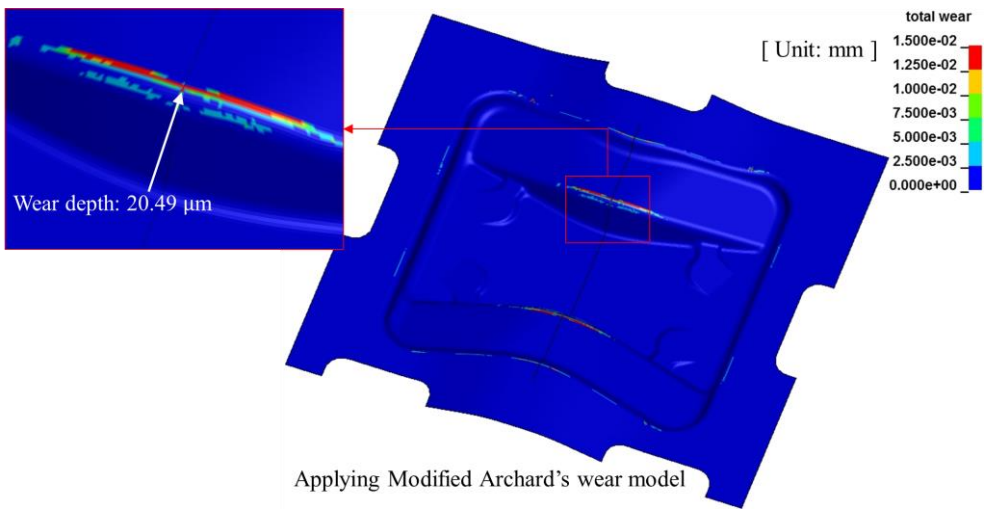

Fig. 5-5. Predicted wear depth distributions on the die after 20,000 strokes (Applying the Modified Archard's wear model)

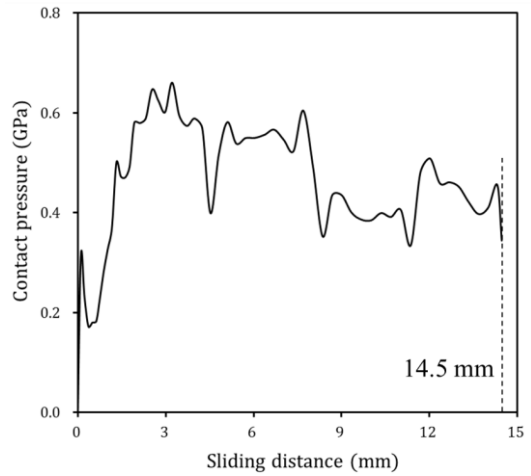

Fig. 5-6. Contact conditions at the die corner where the maximum wear depth is predicted

The Archard's wear model was compared with the Modified Archard's wear model to confirm the limitations of predicting evolutionary wear behavior in forming the automotive parts. As shown in Fig. 5-7, the distributions of the predicted wear depth after 20,000 strokes are illustrated by applying the Archard's wear model to the forming the automotive part. The maximum wear depth was predicted to be 6.57 μm at the die corner with a curvature radius of 7.2 mm. Fig. 5-8 compared the evolutionary wear behaviors with respect to the strokes when applying the tool wear models to forming the automotive part. The modified Archard's wear model can express the evolutionary wear behavior with respect to the number of strokes. However, the wear behavior predicted by the Archard's wear model is linear. It can be observed that wear depth predicted by the Archard's wear model in terms of

the number of strokes significantly differed from that predicted by the Modified Archard's wear model. In addition, the simulation results based on the modified Archard's wear model demonstrated no wear at 5,000 and 10,000 strokes (i.e. before failure). Therefore, the Archard's wear model has limitations in simulating non-linear wear behavior of the tool in sheet metal forming.

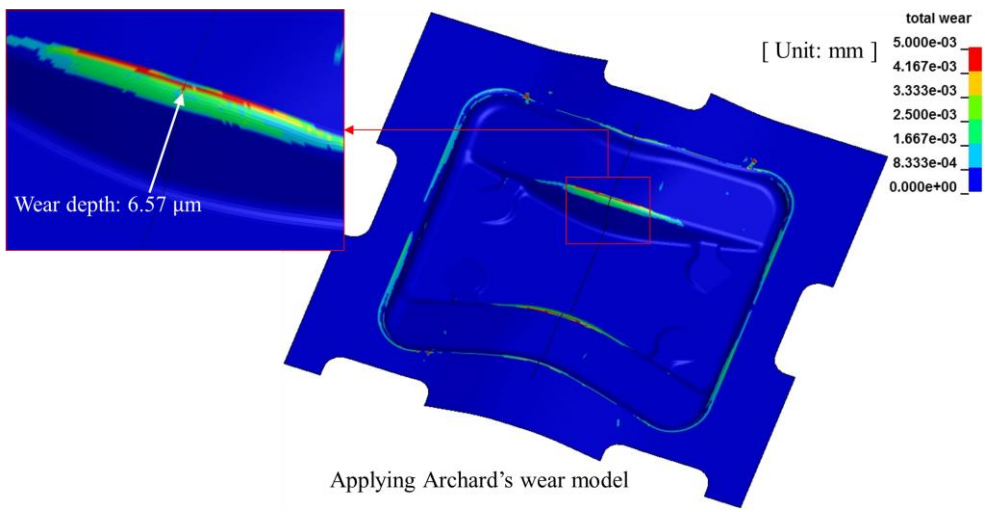

Fig. 5-7. Predicted wear depth distributions on the die after 20,000 strokes (Applying the Archard's wear model)

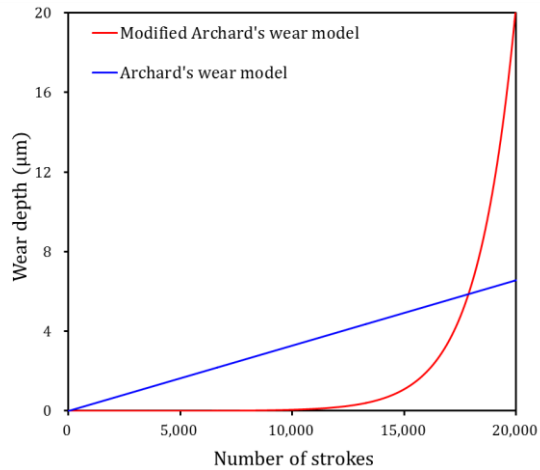

Fig. 5-8. The evolutionary wear behaviors with respect to the strokes when applying the tool wear models to forming the automotive part

6. Conclusion

The first objective of this study is to develop a continuous wear test methodology for quantifying tool wear during the stamping of a 1.2-mm-thick uncoated TRIP1180 steel sheet. A progressive die set was used to enable continuous sheet metal stamping at a consistent work rate and designed to test four different types of punches simultaneously. For efficient and economical wear testing, a rolled steel coil was used, which saved raw materials and specimen production costs. The wear test was made systematic using an uncoiler, automatic feeding system, and press system. The punches used in the wear test were designed to mimic the curvature geometry of the stamping tool used to manufacture the automotive components. The tool wear characteristics are quantified using a variety of parameters, including tool material, punch shape, and coating condition. The following are the conclusions drawn from the study:

- The proposed method is appropriate for performing wear tests on tools manufactured under a variety of conditions, including tool materials, punch shapes, and coatings.
- The wear depth of the punch is close to 0, and the roughness of the punch is also comparable to that of the as-produced prior to failure.

When severe wear occurs, the depth of the wear and roughness of the punch rapidly increase.

- Prior to failure, micro-scratches on the punch surface (plowing mechanism) do not degrade the punch quality. However, worn punches develop a very rough surface on the stamped product.
- Wear of coated tool is caused by the fretting wear mechanism when stamping uncoated steel sheets.
- The measured wear depth is consistent with the wear state represented by the surface roughness and imaging. Thus, the proposed quantitative tool wear evaluation methods are appropriate for establishing a reliable tool wear database.

The second objective of this study is to develop an efficient wear simulation method for predicting quantitative wear reasonably in reduced computational time. The following conclusions are drawn from the results of this study.

- By considering the punch wear characteristics, a nonlinear equation from a modified form of Archard's wear model was proposed to predict the nonlinear wear behavior considering punch shapes (contact pressure) and coating hardness.
- The proposed wear model is suitable for predicting the rapidly

increasing wear depth behavior after failure and determining the number of strokes required to achieve the desired wear depth.

- The modified Archard's wear model was more accurate in predicting nonlinear wear behavior than the Archard's wear model in cold stamping of ultra-high strength steel sheets.
- The geometry update and accumulated wear from the previous iteration of the wear simulation are rendered unnecessary by utilizing the scale factor when implementing the wear simulation method. Thus, the proposed method can decrease the computational time required for the simulation.
- It was revealed that the tool wear in the stamping process degrades the shape accuracy of the formed products.

Reference

[1] A. Jambor, M. Beyer, New cars—new materials, Materials & Design. 18 (1997) 203–209.

[2] S.S. Cheon, D.G. Lee, K.S. Jeong, Composite side door impact beams for passenger cars, Composite Structures. 38 (1997) 29–39.

[3] A.I. Taub, A.A. Luo, Advanced lightweight materials and manufacturing processes for automotive applications, MRS Bulletin. 40 (2015) 1045–1054.

[4] H. Safari, H. Nahvi, M. Esfahanian, Improving automotive crashworthiness using advanced high strength steels, International Journal of Crashworthiness. 23 (2018) 645–659.

[5] C. Lesch, N. Kwiaton, F.B. Klose, Advanced high strength steels (AHSS) for automotive applications – tailored properties by smart microstructural adjustments, Steel Research International. 88 (2012) 1700210.

[6] M.P. Pereira, W. Yan, B.F. Rolfe, Wear at the die radius in sheet metal stamping, Wear. 274–275 (2012) 355–367.

[7] B. Podgornik, J. Jerina, Surface topography effect on galling resistance of coated and uncoated tool steel, Surface and Coatings Technology. 206 (2012) 2792–2800.

[8] B. Podgornik, S. Hogmark, O. Sandberg, Influence of surface roughness and coating type on the galling properties of coated forming tool steel, Surface and Coatings Technology. 184 (2004) 338–348.

[9] A. Gonzalez-Pociño, F. Alvarez-Antolin, J. Asensio-Lozano, Improvement of adhesive wear behavior by variable heat treatment of a tool steel for sheet metal forming, Materials. 12 (2019) 2831.

[10] O. Ogunbiyi, T. Jamiru, R. Sadiku, O. Adesina, O.S. Adesina, B.A. Obadele, Spark

plasma sintering of graphene-reinforced Inconel 738LC alloy: Wear and corrosion performance, Metals and Materials International. 28 (2022) 695–709.

[11] E. Büyükkayacı, İ. Şimşek, D. Özyürek, Influence of mechanical alloying time on microstructure and wear behaviors of Fe–Cu–C alloy, Metals and Materials International. 27 (2021) 4618–4625.

[12] H. Sıralı, D. Şimşek, D. Özyürek, Effect of Ti content on microstructure and wear performance of TZM alloys produced by mechanical alloying method, Metals and Materials International 27 (2021) 4110–4119.

[13] R.G. Woodward, A. Toumpis, A. Galloway, The influence of tempering and annealing on the microstructure and sliding wear response of G350 grey cast iron, Wear. 496–497 (2022) 204283.

[14] Y. Hou, W. Zhang, Z. Yu, S. Li, Selection of tool materials and surface treatments for improved galling performance in sheet metal forming, International Journal of Advanced Manufacturing Technology. 43 (2009) 1010–1017.

[15] A. Ghiotti, S. Bruschi, Tribological behaviour of DLC coatings for sheet metal forming tools, Wear. 271 (2011) 2454–2458.

[16] Ö.N. Cora, K. Namiki, M. Koç, Wear performance assessment of alternative stamping die materials utilizing a novel test system, Wear. 267 (2009) 1123–1129.

[17] E. van der Heide, A.J. Huis in ‘t Veld, D.J. Schipper, The effect of lubricant selection on galling in a model wear test, Wear. 251 (2001) 973–979.

[18] P. Groche, M. Christiany, Evaluation of the potential of tool materials for the cold forming of advanced high strength steels, Wear 302 (2013) 1279–1285.

[19] L.B. Zhao, N. Lin, X.Q. Han, C. Ma, Z.Y. Wang, Y.H. He, Influence of microstructure evolution on mechanical properties, wear resistance and corrosion resistance of Ti(C,N)-based cermet tools with various WC additions, Metals and

Materials International. 27 (2021) 2773–2781.

[20] W. Wang, Y, Zhao, Z. Wang, M. Hua, X. Wei, A study on variable friction model in sheet metal forming with advanced high strength steels, Tribology International. 93 (2016) 17–28.

[21] S. Dou, J. Xia, Analysis of sheet metal forming (stamping process): A study of the variable friction coefficient on 5052 aluminum alloy, Metals. 9 (2019) 853.

[22] C. Wang, J. Chen, Z.C. Xia, F. Ren, Die wear prediction by defining three-stage coefficient K for AHSS sheet metal forming process, International Journal of Advanced Manufacturing Technology. 69 (2013) 797–803.

[23] P. Carlsson, U. Bexell, M. Olsson, Friction and wear mechanisms of thin organic permanent coatings deposited on hot-dip coated steel, Wear. 247 (2001) 88–99.

[24] J. Bang, N. Park, J. Song, H.-G. Kim, G. Bae, M.-G. Lee, Tool wear prediction in the forming of automotive DP980 steel sheet using statistical sensitivity analysis and accelerated U-Bending based wear test, Metals. 11 (2021) 306.

[25] Ö.N. Cora, M. Koç, Experimental investigations on wear resistance characteristics of alternative die materials for stamping of advanced high-strength steels (AHSS), International Journal of Machine Tools and Manufacture. 49 (2009) 897–905.

[26] A. Gåård, P.V. Krakhmalev, J. Bergström, N. Hallbäck, Galling resistance and wear mechanisms – cold work tool materials sliding against carbon steel sheets, Tribology Letters. 26 (2007) 67–72.

[27] A. Gåård, P. Krakhmalev, J. Bergström, Wear mechanisms in deep drawing of carbon steel – correlation to laboratory testing, Tribotest. 14 (2008) 1–9.

[28] E. van der Heide, E.D. Stam, H. Giraud, G. Lovato, N. Akdut, F. Clarysse, P. Caenen, I. Heikillä, Wear of aluminium bronze in sliding contact with lubricated stainless steel sheet material, Wear. 261 (2006) 68–73.

[29] E. van der Heide, M. Burlat, P.J. Bolt, D.J. Schipper, Wear of soft tool materials iin sliding contact with zinc-coated steel sheet, Journal of Materials Processing Technology. 141 (2003) 197–201.

[30] C. Hoher, D. Attaf, L. Penazzi, C. Levaillant, Wear behaviour on the radius portion of a die in deep-drawing: Identification, localisation and evolution of the surface damage, Wear. 259 (2005) 1097–1108.

[31] M. Eriksen, The influence of die geometry on tool wear in deep drawing, Wear. 207 (1997) 10–15.

[32] M.J. Alinger, C.J. Van Tyne, Evolution of die surfaces during repeated stretch-bend sheet steel deformation, Journal of Materials Processing Technology. 141 (2003) 411–419.

[33] P. Groche, G. Nitzsche, A. Elsen, Adhesive wear in deep drawing of aluminum sheets, CIRP Annals. 57 (2008) 295–298.

[34] D. Hortig, D. Schmoeckel, Analysis of local loads on the draw die profile with regard to wear using the FEM and experimental investigations, Journal of Materials Processing Technology. 115 (2001) 153–158.

[35] T. Sato, T. Besshi, Anti-galling evaluation in aluminum sheet forming, Journal of Materials Processing Technology. 83 (1998) 185–191.

[36] M.P. Pereira, W. Yan, B.F. Rolfe, Contact pressure evolution and its relation to wear in sheet metal forming, Wear. 265 (2008) 1687–1699.

[37] E. Schedin, Galling mechanisms in sheet forming operations, Wear. 179 (1994) 123–128.

[38] M.P. Pereira, M. Weiss, B.F. Rolfe, T.B. Hilditch, The effect of the die radius profile accuracy on wear in sheet metal stamping, International Journal of Machine Tools and Manufacture. 66 (2013) 44–53.

[39] A. Nilsson, P. Gabrielson, J.-E. Ståhl, Zinc-alloys as tool materials in short-run sheet-metal forming processes: Experimental analysis of three different zinc-alloys, Journal of Materials Processing Technology. 125–126 (2002) 806–813.

[40] W. Wu, D. Zhou, D.J. Adamski, D. Young, Y. Wang, Evaluation of die wear with stamping DP1180 Steel, Auto/Steel Partnership. (2017), https://www.a-sp.org/wp-content/uploads/2020/08/Track-1-Wu.pdf. Accessed 22 May 2017.

[41] H. Hoffmann, C. Hwang, K. Ersoy, Advanced wear simulation in sheet metal forming, CIRP Annals. 54 (2005) 217–220.

[42] K. Ersoy-Nürnberg, G. Nürnberg, M. Golle, H. Hoffmann, Simulation of wear on sheet metal forming tools—An energy approach, Wear. 265 (2008) 1801–1807.

[43] M.P. Pereira, W. Yan, B.F. Rolfe, Sliding distance, contact pressure and wear in sheet metal stamping, Wear. 268 (2010) 1275–1284.

[44] J.A. Williams, Wear modelling: analytical, computational and mapping: a continuum mechanics approach, Wear. 225–229 (1999) 1–17.

[45] K. Hokkirigawa, K. Kato, An experimental and theoretical investigation of ploughing, cutting and wedge formation during abrasive wear, Tribology International. 21 (1988) 51–57.

[46] R.B. Waterhouse, Fretting fatigue, International Materials Reviews. 37 (1992) 77–98.

[47] A.A.Voevodin, T. Liskiewicz, N. Laugel, A. Yerokhin, Surface characteristics underpinning fretting wear performance of heavily loaded duplex chameleon/PEO coatings on Al, Tribology International. 154 (2021) 106723.

[48] J. Xu, M.H. Zhu, Z.R. Zhou, Ph. Kapsa, L. Vincent, An investigation on fretting wear life of bonded MoS_2 solid lubricant coatings in complex conditions, Wear. 255 (2003) 253–258.

[49] A. Tricoteaux, P.Y. Jouan, J.D. Guerin, J. Martinez, A. Djouadi, Fretting wear properties of CrN and Cr_2N coatings, Surface and Coatings Technology. 174–175 (2003) 440–443.

[50] L. Cunha, M. Andritschky, K. Pischow, Z. Wang, Microstructure of CrN coatings produced by PVD techniques, Thin Solid Films. 355–356 (1999) 465–471.

[51] H. Zhou, J. Zheng, B. Gui, D. Geng, Q. Wang, AlTiCrN coatings deposited by hybrid HIPIMS/DC magnetron co-sputtering, Vacuum. 136 (2017) 129–136.

[52] R. Hill, A theory of the yielding and plastic flow of anisotropic metals, Proceedings of the Royal Society of London. Series A. Mathematical and Physical Sciences. 193 (1948).

[53] S.K. Rhee, Wear equation for polymers sliding against metal surfaces, Wear. 16 (1970) 431–445.

[54] R.G. Bayer, A general model for sliding wear in electrical contacts, Wear. 162–164 (1993) 913–918.

[55] J.F. Archard, Contact and rubbing of flat surfaces, journal of Applied Physics. 24 (1953) 981–988.

[56] P. Põdra, S. Addersson, Simulating sliding wear with finite element method, Tribology International. 32 (1999) 71–81.

Korean abstract

자동차는 연비 효율성 및 승객의 충돌안전성 향상을 위해 차체의 경량화 및 충돌성능을 만족해야 한다. 초고장력강판의 적용은 차체의 생산비용 절감 및 충돌에너지 흡수 성능을 향상할 수 있다. 그러나 초고장력강판의 성형 시 일반적으로 사용되는 판재보다 더 높은 성형 반력으로 인해 예상보다 이른 금형마모를 유발하며 이로 인한 다양한 문제점들을 야기시킨다. 따라서, 프레스 성형 공정에서 금형마모를 정량화하기 위한 효율적인 마모 실험방법 및 예측 기법이 필요하다.

본 연구에서는 판재 성형공정에서 금형마모를 정량화 할 수 있는 실험적 방법 및 해석의 연산 속도를 줄이면서 비선형 마모거동을 예측할 수 있는 효율적인 금형마모 해석 프로세스를 개발하는 것을 목표로 한다. 일정한 성형속도로 연속 판재성형이 가능하며, 실험 시간과 비용 면에서 효율적인 프로그레시브 금형을 금형마모 실험에 사용하였다. 설계된 금형은 다양한 금형강종, 금형형상, 코팅과 같은 다양한 조건으로 제작된 네 가지 펀치 금형을 동시에 실험할 수 있도록 설계하였다. 펀치의 형상은 자동차 부품 성형 금형에서 마모 민감 형상을 모사하여 설계하였다. 금형의 마모깊이 그리고 금형과 제품의 표면거칠기를 정량적으로 측정하여 금형마모를 평가하였다. 제품의 표면에 스크레치로

인한 품질 저하가 발생하기 전까지 금형은 미세한 스크레치는 관찰되었지만 극심한 마모는 발생하지 않았으며, 표면 프로파일 변화는 없었다. 하지만 제품 표면 품질이 저하되었을 때 금형 표면의 마모깊이 및 표면거칠기가 급격하게 증가하였다. 마모실험 결과를 바탕으로 마모 특성을 분석하여 프레팅 마모가 비도금강판의 성형공정에서 주요한 마모 메커니즘인 것을 확인하였으며, 제안된 금형마모 실험방법이 금형의 내마모 성능을 정량적으로 평가하고 마모 특성 및 메커니즘을 분석하기에 적합한 것을 확인하였다. 이러한 비선형 마모거동을 예측하기 위해, 아차드 마모모델을 변형한 수정 아차드 마모모델을 제안하였다. 수정 아차드 마모모델은 마모계수를 성형 타수의 함수로 구성하여 타수에 따른 비선형 마모거동을 예측할 수 있도록 하였다. 이 모델을 마모 시뮬레이션에 적용하여 이전 성형 타수에서의 마모 시뮬레이션으로부터 금형 형상을 이용한 반복적인 시뮬레이션의 수행을 피할 수 있도록 하였다. 따라서 제안한 마모시뮬레이션 방법은 형상 업데이트를 할 필요가 없기 때문에 연산 시간 측면에서 효율적이다.